PAPER

Check for updates

Concentration-dependent effects of nickel doping on activated carbon biocathodes†

Konstantina-Roxani Chatzipanagiotou, [iD] [ab] Ludovic Jourdin, [iD] [bc] Johannes H. Bitter [iD] *[a] and David P. B. T. B. Strik [iD] *[b]

In microbial electrosynthesis (MES), microorganisms grow on a cathode electrode as a biofilm, or in the catholyte as planktonic biomass, and utilize CO_2 for their growth and metabolism. Modification of the cathode with metals can improve MES performance, due to their catalytic activity for H_2 production, which can be consumed by microorganisms, or *via* modifying the cathode properties. On the other hand, metals can have an inhibiting effect on MES. While these single roles of metals and their oxides have been identified, an investigation of the simultaneous effects on MES is still lacking. Here, we modify activated carbon (AC) electrodes with nickel (Ni) at high (5%) and low (0.01%) loadings, to investigate its combined effects on MES. Upon Ni impregnation, multiple factors explained the MES performance, including electrocatalytic H_2 production, trace element availability, metal toxicity, Ni leaching and redeposition/bio-crystalization. Instead, the electrode surface properties (*i.e.*, surface area and pore structure) were not affected by Ni addition. Compared to unmodified AC, low Ni loading did not improve abiotic H_2 production, whereas at high Ni loading a 6-fold increase was observed. During biological experiments, low Ni loading resulted in over a 3-fold increase of acetate production and 35% higher planktonic growth, compared to unmodified AC. Instead, high Ni loading resulted in 25-fold increase of acetate production, 21% decrease of planktonic growth, and improved biofilm growth. Unmodified AC, and low and high Ni loading each resulted in unique microbial community composition. The effect of Ni on MES is therefore concentration-dependent, with apparently different mechanisms of interaction being prevalent at low or high Ni loadings.

Introduction

Globally, there are ongoing efforts to decrease carbon dioxide (CO_2) emissions. CO_2 can be converted to valuable products *via* chemical or biological conversion. Microbial electrosynthesis (MES) is an electrocatalytic conversion process based on the ability of microorganisms to reduce CO_2 to products such as methane (CH_4), acetate and ethanol, in the presence of a cathode electrode. During MES, an oxidation reaction takes place at the anode, releasing protons and electrons. These are transferred to the cathode and utilized by microorganisms to catalyse the reduction of CO_2 into organic molecules.[1] MES can be performed using either pure cultures or mixed cultures of different microorganisms. Microorganisms can grow in suspension (planktonic microorganisms) or as biofilm on the electrode surface.[2] Direct electron transfer from the cathode to the microorganisms is facilitated by biological structures such as c-type cytochromes, quinones, ferredoxin complexes and electroconductive pili.[1,3] Aside from direct electron transfer, which is limited to truly electroactive species, indirect electron mediators (*e.g.*, methyl viologen, anthraquinone-2,6-disulfonate and neutral red) and/or electrochemically produced electron donors such as hydrogen (H_2) can also be used during MES.[4]

Metals and their oxides have a plurality of (potential) roles which can affect microbial growth and metabolism, as reviewed in Table 1. In an attempt to improve the performance of MES, electrode modification with metals has been proposed. Metals can enhance electron transfer between the electrode and the biofilm, due to their low charge-transfer resistances and high conductivities. In addition, metal nanostructures have been proposed to enhance biofilm attachment to the electrode, due to their high active surface area and biocompatibility.[5] For example, adding iron oxide

[a] Biobased Chemistry and Technology, Wageningen University & Research, Bornse Weilanden 9, 6708 WGWageningen, The Netherlands. E-mail: harry.bitter@wur.nl

[b] Environmental Technology, Wageningen University & Research, Bornse Weilanden 9, 6708 WGWageningen, The Netherlands. E-mail: david.strik@wur.nl

[c] Department of Biotechnology, Delft University of Technology, van der Maasweg 9, 2629 HZDelft, The Netherlands

† Electronic supplementary information (ESI) available. See DOI: 10.1039/d1cy02151f

2500 | *Catal. Sci. Technol.*, 2022, **12**, 2500–2518

This journal is © The Royal Society of Chemistry 2022

Table 1 Mechanisms of interaction between metals/metal oxides and microorganisms

Role of metal	Explanation of interaction mechanism
Electrode modifier	Increased surface area and roughness for improved biofilm coverage and attachment[5,7]
	Increased electron conductivity and decreased charge-transfer resistance for improved electron transfer to biofilm-forming microorganisms[5–7,11]
Electrocatalyst	Electrocatalytic production by the metal catalyst of electron donors (e.g., H_2) that can be oxidized by microorganisms in the biofilm or in the planktonic phase[8,9]
Trace element	Increased availability of a certain trace element (i.e., added metal) that can improve microbial growth (in case the concentration was limiting)[12,13] or alter the enzymatic pathways[14] and/or microbial community composition[15,16]
Toxic compound	Inhibition of microbial growth or altered microbial community composition via inhibition of metal-sensitive taxa due to high metal concentration[17,18]

on granular activated carbon cathodes has been shown to increase current density and acetate production, by increasing extracellular electron transfer and resulting in an enrichment of iron-reducing microorganisms.[6] Adding gold, palladium or nickel nanoparticles on a carbonaceous cathode during MES increased the current density and acetate production versus a control without metals.[5] Furthermore, a nickel nanowire-coated graphite electrode improved the current density, acetate production and biofilm formation, compared to a control electrode.[7] This has been attributed to the increased electron-exchange capacity and conductivity of the nickel-modified electrode. Furthermore, the surface roughness and porosity of the electrode increased via nickel addition, which improved biofilm attachment.[7]

Next to these indirect effects on the growth and biocatalytic activity of microorganisms (via the electrode properties), metals and their oxides can also have a more direct effect on microbial metabolism, via their electrocatalytic activity, such as the electrocatalytically-produced H_2, which can be consumed by microorganisms. For example, Tian and co-workers showed that a H_2-producing molybdenum carbide electrocatalyst on graphite felt electrodes, combined with mixed-culture MES, resulted in improved acetate production and biofilm formation, due to the electrocatalytic activity of the added metal.[8] Kracke and co-workers combined H_2-producing electrocatalysts (cobalt-phosphide, molybdenum-disulfide and nickel–molybdenum alloy electrodes) with acetate and methane-producing microorganisms, and report that the microorganisms in suspension were able to fully utilize the electrocatalytically-produced H_2 as an electron donor for the production of acetate and methane.[9] Metal electrocatalysts for H_2 production have also been used to improve the methane production of hydrogenotrophic methanogens in coupled anaerobic digestion and microbial electrolysis reactors. For example, Wang and co-workers used stainless steel, copper and nickel mesh electrodes as biocathodes, and report higher methane production with nickel, presumably due to the higher electrocatalytic activity of this electrode for H_2 production.[10] Thus, metal electrocatalysts can have a direct effect on improving the production rate of biological reactions, by catalysing the production of substrates (e.g., H_2), which can be thereafter used by microorganisms as a substrate for biological reactions (e.g., CO_2 reduction during MES).

While both the indirect (e.g., surface properties) and direct effects (e.g., H_2 production) of nickel nanostructures on MES are well known and described separately, the combination of these effects on MES has been overlooked during previous studies. For example, during studies on the effect of metals on the surface and electron transfer properties of the electrode,[5–7] the authors did not report abiotic testing of the synthesized cathodes, which would have revealed whether H_2 production was enhanced due to metal addition, thus leading to improved acetate production by the microorganisms. Similarly, during studies on the catalytic activity of metals and its effect on MES,[8] the authors correlated the improved acetate production solely to the H_2 production, without reporting the effect of the metal on the surface properties of the electrode. Finally, aside from the direct and indirect effects discussed so far in relation to MES, another direct effect of metals on microbial growth and metabolism is the availability of the tested metals as trace elements, and the potentially inhibiting effect of high metal concentration on biological processes.[19,20] However, these two mechanisms of interaction between metals/metal oxides and MES have also been previously overlooked.

Among the metals tested for electrode modification during MES, nickel is of particular interest, as it can have multiple roles in bio-electrochemical processes. Nickel is an essential trace element,[21] while it can be toxic at high concentrations,[19,20] and it has been previously shown to catalyse the production of H_2 at high rates as a cathode electrode.[22] Therefore, in order to elucidate the effect of nickel addition on MES, all the potential roles of nickel ought to be considered. Aside from the specific metal used, the amount of metal should also be taken into account, as this would likely affect the mechanism of interaction with microorganisms. Studies on the concentration-dependent effect of nickel on MES, which could reveal the prevalent mechanism of interaction between nickel and microorganisms, are lacking. Instead, the concentration-dependent effect of iron oxide on the extracellular electron transfer and enrichment of electroactive microorganisms has been previously shown during MES studies.[6] However, different mechanisms of interaction depending on the iron loading were not reported, and a concentration-dependent effect was solely correlated to the dispersion of iron oxide nanoparticles.[6]

This journal is © The Royal Society of Chemistry 2022

Catal. Sci. Technol., 2022, **12**, 2500–2518 | **2501**

Here, we report on a comparative MES performance study using high (*i.e.*, 5%), low (*i.e.*, 0.01%) and no nickel loading on a carbonaceous cathode. The surface properties (*i.e.*, surface area and porosity), electrocatalytic activity for H_2 production and metal leaching of the three cathodes were measured, and correlated to various parameters of MES performance (product formation, microbial growth and microbial community composition). We show for the first time that the mechanism of interaction between nickel and MES depends on the amount of added metal. Doping AC granules with nickel at both high and low loadings resulted in an overall improvement of acetate production with MES, albeit *via* apparent different mechanisms. Upon nickel doping on the cathode, the main factors influencing the MES performance were H_2 production, current density and nickel concentration. No clear correlation could be observed between MES performance and surface properties of the electrode (*i.e.*, surface area and pore structure), indicating a negligible role in this study. Overall, this study reveals the importance of a multi-factorial approach to elucidate the different mechanisms of interaction between metals and MES, including both direct and indirect effects of metal doping on the cathode electrode.

Experimental

Electrode preparation

Granular activated carbon (AC, PK 3–5, from Sigma-Aldrich) was pre-oxidised in 32% nitric acid aqueous solution at 25 °C overnight, to ensure the formation of oxygen groups on the surface, which allow anchoring of the metal. AC granules were loaded with nickel nitrate hexahydrate (Sigma-Aldrich) dissolved in demineralised water, *via* incipient wetness impregnation. After impregnation, materials were first dried at 105 °C overnight, followed by calcination at 200 °C for two hours in a static air oven (Nabertherm P 330, Germany), forming nickel oxide.[22] Two target metal loadings were selected in this study: low nickel loading at 0.01% wt (sample AC-Ni 0.01%) and high nickel loading at 5% wt (sample AC-Ni 5%). Control/blank AC granules were also prepared using the same treatments but without addition of the metal salt (sample control).

To prepare the working cathode electrodes, AC granules were manually compressed in a perforated polypropylene tube (Sibel, 5 cm height, 1.35 cm inner diameter), with a titanium wire core serving as current collector (Ø = 1 mm). For all electrodes prepared, the average resistivity was <1 Ω between the current collector and different positions of the AC granules in the polypropylene tube. The amount of AC added per electrode was on average 0.990 ± 0.001 g for the control, 0.990 ± 0.020 g for the AC-Ni 0.01% and 1.110 ± 0.086 g for the AC-Ni 5%. Counter electrodes were prepared by wrapping 7 cm of platinum wire (Ø = 0.3 mm) around a titanium wire current collector. The reference electrode used for all electrochemical tests was Ag/AgCl (3 M KCl), and all potentials in this paper are reported against that electrode.

Electrochemical reactor operation and product analysis

Chronoamperometry experiments at a cathode potential of −1.06 V *vs.* Ag/AgCl (*i.e.*, −0.85 V *vs.* SHE) were performed in 3-electrode, 2-compartment electrochemical H-type reactors as previously described.[23] A Nafion cation-exchange membrane (projected surface area 11.3 cm^2) separated the anode and cathode compartments. The anolyte (250 ml) was phosphate buffer (6 g L^{-1} Na_2HPO_4, 3 g L^{-1} KH_2PO_4, pH 6.7). The catholyte (230 ml) was autoclaved biological growth medium of the following composition: 0.2 g L^{-1} NH_4Cl, 0.04 g L^{-1} $MgCl_2 \cdot 6H_2O$, 0.015 g L^{-1} $CaCl_2$, 6 g L^{-1} Na_2HPO_4, 3 g L^{-1} KH_2PO_4, 2.11 g L^{-1} $BrCH_2CH_2SO_3Na$ and 1 ml L^{-1} of mixed trace element solution. The trace element solution contained: 1.5 g L^{-1} $FeCl_3 \cdot 6H_2O$, 0.15 g L^{-1} H_3BO_3, 0.03 g L^{-1} $CuSO_4 \cdot 5H_2O$, 0.18 g L^{-1} KI, 0.12 g L^{-1} $MnCl_2 \cdot 4H_2O$, 0.06 g L^{-1} $Na_2MoO_4 \cdot 2H_2O$, 0.12 g L^{-1} $ZnSO_4 \cdot 7H_2O$, 0.15 g L^{-1} $CoCl_2 \cdot 6H_2O$, 0.023 g L^{-1} $NiCl_2 \cdot 6H_2O$, and 10 g L^{-1} EDTA.

Microorganisms were harvested from a parent reactor with a graphite felt cathode electrode (4 mm thick, CTG carbon GmbH, Germany) which has been operated for three years to produce volatile fatty acids from CO_2 in an electrochemical reactor as described in the paragraph above. Microorganisms growing in the parent reactor were provided from a previously described acetate-producing mixed culture biocathode.[24] A liquid sample was taken from the parent reactor, centrifuged twice, re-suspended in fresh biological growth medium and used as inoculum. At the time of inoculation, the concentration of the major liquid products in the parent reactor was approximately 5 g L^{-1} acetate and 1 g L^{-1} *n*-butyrate, whereas gas products were not monitored.

All electrochemical tests were performed at 25 °C. The catholyte was flushed with CO_2 prior to each experiment for one hour, and the pH was approximately 6.7 after flushing. A multi-layer foil gas bag (Cali-5-Bond™) was connected to the headspace of each reactor and was used to collect gaseous products. Liquid and gas samples were analysed every 2–3 days (*i.e.*, 3 times per week). After sampling, the catholyte was replenished with an equal volume (10–15 ml) of fresh medium and flushed with CO_2 for 30 minutes. An IVIUM n-stat potentiostat (IVIUM, Netherlands) was used for all electrochemical experiments.

Gas chromatography (Agilent Technologies) with flame ionization detector (GC-FID) was used to analyse liquid products from chronoamperometry experiments (C2–C8 carboxylic acids, C1–C6 alcohols), as previously described.[25] Gas chromatography was also used to analyse the gas composition (O_2, N_2, CO_2, H_2, CH_4, CO), as previously described.[26] The concentration of formate was measured with high performance liquid chromatography (HPLC), with refractive index and UV detection (column specification: Aminex HPX-87H, 300 × 7.8 mm, BioRad 1225-0140). Prior to GC and HPLC analysis, samples were filtered with a 0.45 μm cellulose acetate syringe filter.

Analysis of electrodes and microbial community composition

At the end of MES experiments, electrodes were removed from the reactor and allowed to dry under N_2 flow. The

2502 | *Catal. Sci. Technol.*, 2022, **12**, 2500–2518

This journal is © The Royal Society of Chemistry 2022

Table 2 BET surface area, t-plot external surface area, t-plot micropore (≤ 1 nm) area and metal loading of AC granules

Sample	BET surface area ($m^2\ g^{-1}$)	External surface area ($m^2\ g^{-1}$)	Micro-pore area ($m^2\ g^{-1}$)	Ni (wt%)	Fe (wt%)
Control	663 ± 30	209 ± 12	454 ± 22	0.0	1.3×10^{-1}
AC-Ni 0.01%	676 ± 15	190 ± 2	485 ± 17	1.7×10^{-2}	8.2×10^{-2}
AC-Ni 5%	665 ± 7	168 ± 26	498 ± 33	6.3	7.7×10^{-2}

biocathodes were dried in whole before individual granules were removed from the polypropylene tube, to prevent scraping off the biofilm. Once dried, the granules were immediately harvested for characterization.

Part of the sample was transferred into a 2.5% glutaraldehyde solution to fixate biological structures prior to characterization with scanning electron microscopy (SEM). SEM was performed using a FEI Magellan 400 FESEM with energy dispersive X-ray spectroscopy (EDX) (Oxford Instruments). EDX was performed using an Everhart–Thornley detector, at 2.00 kV voltage and 13 pA current. SEM-EDX analysis was performed on both unused and biofilm-covered AC granules. In addition, transmission electron microscopy (JEM-1400Plus) analysis was performed on unused AC-Ni 5% granules, to visualize nickel structures.

The metal loading of AC samples was measured *via* inductively coupled plasma optical emission spectroscopy (ICP-OES; Perkin Elmer ICP-OES AVIO 500). For ICP-OES measurements, microwave-assisted extraction in aqueous HNO_3 and HCl solution was used to dissolve all metals from the carbonaceous support. Textural properties of samples were assessed using nitrogen physisorption (Micromeritics Tristar II PLUS) at liquid nitrogen temperature. Prior to physisorption measurements, the samples were degassed at 120 °C for 12 h (Micrometrics VacPrep 061). For the calculations of the isotherm data plots, the BET (Brunauer–Emmett–Teller) method was used and the pressure region for fitting the linearized data was determined by the Rouquerol method.

To assess the microbial community composition, at the end of MES experiments, liquid samples (40 ml) were removed from each reactor and centrifuged. The pellet formed after centrifugation was transferred in an Eppendorf tube, immersed in liquid N_2, and stored at −80 °C. DNA extraction, amplification, and taxonomic analysis was performed on these samples using next generation sequencing (NGS) as previously described.[27] In order to estimate the deviation among duplicate reactors, for all three electrode types, DNA sample was acquired from each of the duplicate reactors and analysed separately. During the inoculum preparation for MES experiments, a pellet sample from the parent reactor was also acquired and subjected to the same procedure, in order to assess the microbial community composition of the parent reactor. NGS sequences were deposited in the European Nucleotide Archive.‡ Other raw experimental data related to electrode characterization and

reactor operation are available in the 4TU.ResearchData repository.§

Calculations and statistical analysis

The current densities (in mA cm^{-3}) reported throughout this manuscript were calculated based on the apparent volume of the electrode. This volume was calculated ($V = \pi \cdot r^2 \cdot h$) based on the dimensions of the cylindrical electrodes ($r = 0.675$ cm and $h = 5$ cm), and corresponds to 7.157 cm^3 for all electrodes tested.

The total amount of nickel on each electrode was calculated based on the metal loading measured with ICP-OES (in %, Table 2), multiplied by the average amount of AC of each electrode (in gram, given in Electrode preparation section). Leaching of nickel in the electrolyte during experiments was calculated based on the amount of dissolved nickel (likely as nickel oxide) in the catholyte, measured with ICP-OES (in μg L^{-1}), excluding the amount of nickel present in fresh electrolyte, and expressed as percentage of the total amount of nickel on each electrode.

For electrochemical experiments, electron recovery (%) was calculated between consecutive sampling points (*i.e.*, with a time interval of 48 or 72 hours). The produced amount of gas and liquid products (in mol) was calculated based on the concentration difference between sampling points, as measured with HPLC and GC. The number of electrons (in mol) recovered in the product was estimated based on reaction stoichiometry (*i.e.*, 2 mols of electrons per mol formate and hydrogen, 8 mols of electrons per mol acetate and methane), and converted to electric charge, by multiplying with the Faraday constant (96 485 Coulombs per mol electrons). Electron recovery was calculated as the percentage of electric charge recovered into the product, compared to the total electric charge between two sampling points, as recorded by the potentiostat.

The non-parametric Spearman's rho correlation coefficient (2-tailed) was calculated using SPSS Statistics software (IBM SPSS Statistics 25), to estimate the correlation between the main microbial genera identified with NGS and several parameters measured during MES experiments (*i.e.*, electrocatalytic activity, dissolved nickel oxide concentration, onset of product formation, product concentration and electron recovery, microbial growth). For this analysis, only data corresponding to experimental reactors were used, whereas NGS data from the inoculum samples were not included. One-star significance corresponds to correlations at the 0.05 level, and two-star significance corresponds to correlations at the 0.01 level.

‡ 16S rRNA gene raw sequences are deposited in the ENA database (https://www.ebi.ac.uk/ena, accessed on 1 March 2022) under the accession number PRJEB51246.

§ The datasets generated during the current study are available in the 4TU. ResearchData repository (DOI: 10.4121/19248359, accessed on 9 March 2022).
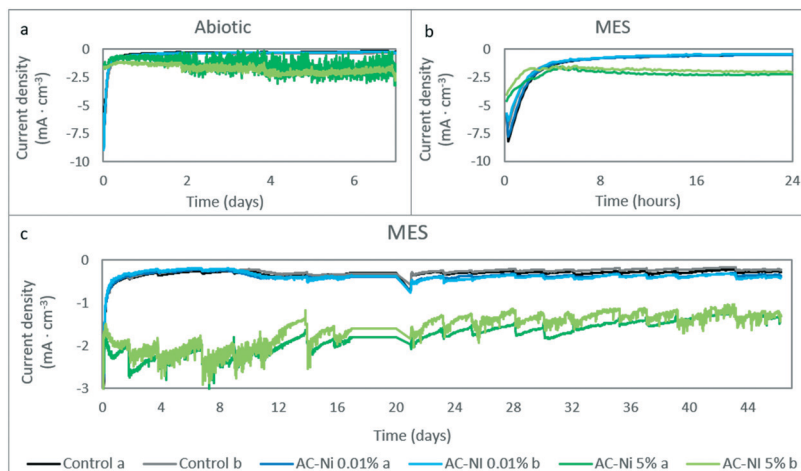
Fig. 1 Current density (mA cm^{-3}) recorded during abiotic (a) and MES experiments (b and c) with the three types of AC electrodes in duplicate experiments. In figure b, the current density for MES experiments is shown for the first 24 hours, to clearly visualize the sharp decrease in current at the start of the experiment. In figure c, the entire duration of MES experiments is shown for a limited range between 0 and −3 mA cm^{-3}, in order to better visualize the deviation among reactors. Due to a technical problem, a power failure occurred in the laboratory for approximately 24 hours on day 20 during MES experiments. As a result, reactors were operating under open cell potential (OCP) during that time (day 20–21), and data regarding the current density between days 17–20 were lost. During that time (day 17–20), a stable value was assumed for the current, calculated as the average current recorded for 1 hour in each reactor before data was lost (evident as a flat line in figure c).

Results

Abiotic and biological (*i.e.*, MES) electrochemical experiments were performed in duplicate, and the results (*i.e.*, current density, product concentration, electron recovery, optical density) are summarized in Fig. 1–4.

Concentration-dependent increase of current density with nickel

The current density (in mA cm^{-3}) over time (in days or hours) during electrochemical experiments with each electrode is shown in Fig. 1a (for abiotic) and b and c (for MES experiments). During cathodic operation, negative values are recorded for the current, and higher cathodic current corresponds to more negative values. For both abiotic and MES experiments, the current density ranged between −9 and −0.1 mA cm^{-3}. During
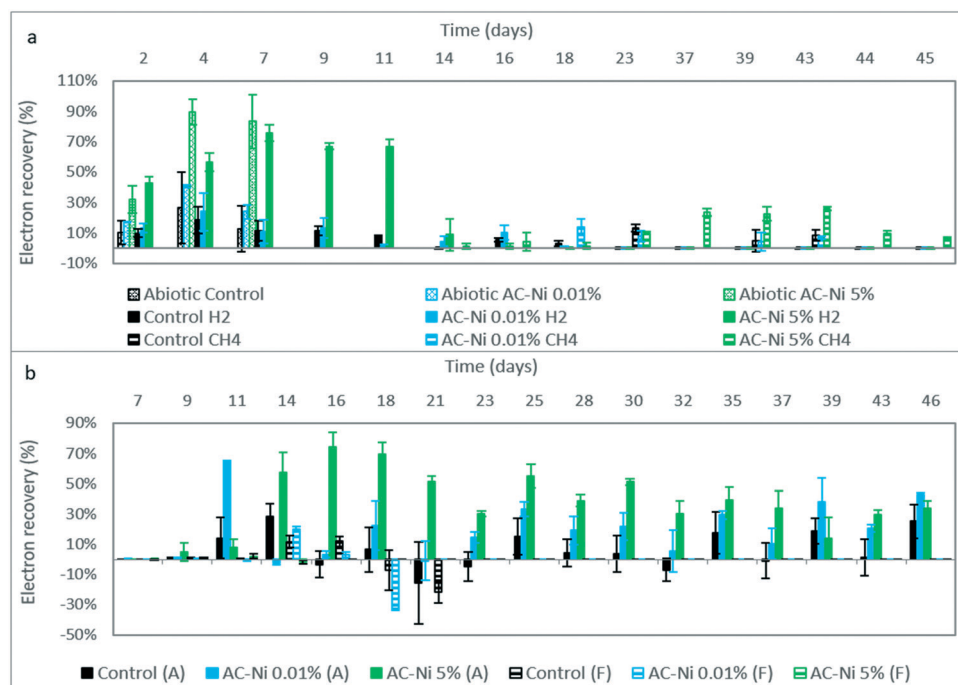
the first minutes of the experiment, the current density was higher (*e.g.*, up to −9 mA cm^{-3} for abiotic AC-Ni 0.01%), and thereafter transitioned to lower values, during both abiotic and MES experiments. After this initial sharp change in current, the current density was more stable for the rest of the experiment. Stable current density after day 1 corresponded to less than −1 mA cm^{-3} for control and low Ni loading electrodes during both abiotic and MES experiments. For high Ni loading a higher cathodic current was measured, *i.e.*, around −2 mA cm^{-3} for both abiotic and MES experiments. In Fig. 1b, the full current range for MES experiments is shown during the first day of the experiment, to illustrate the sharp change in current during the initial phase. For clearer visualization of the long-term current density, only values between −3 and 0 mA cm^{-3} are shown in Fig. 1c.

Previous studies on MES have reported an evolution of the current density towards more negative values over time.[24]
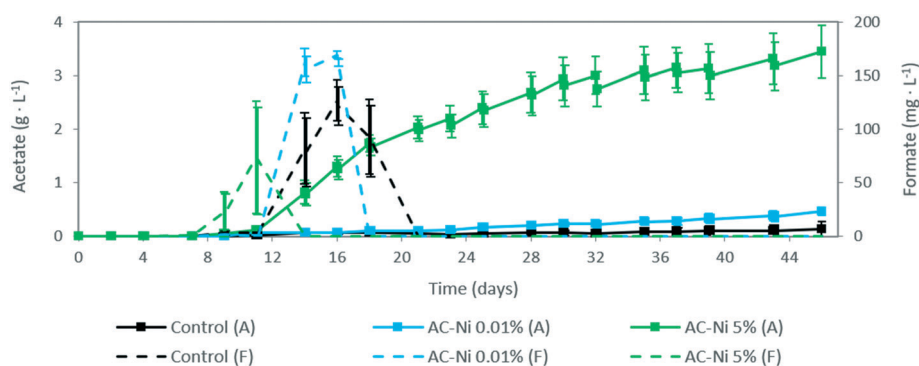
Fig. 2 Average concentration of acetate (A, left axis, in g L^{-1}) and formate (F, right axis, in mg L^{-1}) measured in the electrolyte over time during MES experiments. At each sampling point, both the measured and the calculated concentration after refreshing the electrolyte are shown. Error bars indicate the standard deviation based on duplicate experiments.

2504 | *Catal. Sci. Technol.*, 2022, **12**, 2500–2518

This journal is © The Royal Society of Chemistry 2022

Fig. 3 Average electron recovery (in %) for gas (a) and liquid (b) products over time during abiotic and MES experiments. H_2 was the only product detected during abiotic experiments (graph a), whereas H_2, CH_4 (graph a), acetate (A) and formate (F) (graph b) were produced during MES experiments. Error bars indicate the standard deviation based on duplicate experiments.

Nevertheless, such an effect was not observed in the MES experiments reported here (Fig. 1c). The initial sharp change in current density during the first minutes of the experiment for all electrodes can be attributed to capacitance, as well as reduction of components on the electrode and in the electrolyte at the start of the experiment.[23,28]

While the initial cathodic current density was lower with AC-Ni 5%, compared to the other two electrodes (Fig. 1a and b), this electrode reached a higher current during the rest of the experiment, for both abiotic and MES experiments (Fig. 1a and c, respectively), thus indicating an effect of high Ni loading on the electrocatalytic activity of AC, likely *via* improved H_2 production, as has been previously discussed for carbon electrodes modified with Pt or Ni.[10] Instead, AC-Ni 0.01% and control electrodes reached a

similar current density throughout abiotic electrochemical experiments (Fig. 1a), thus indicating that low Ni loading did not improve the catalytic activity of AC. During MES experiments (Fig. 1c), the current density was not significantly different between control and AC-Ni 0.01% electrodes during the first 20 days. Instead, some deviation could be observed from day 20 onwards (*i.e.*, after a power failure of 24 hours, described in Fig. 1), with an average current density of -0.26 ± 0.04 mA cm^{-3} for control and -0.39 ± 0.02 mA cm^{-3} for AC-Ni 0.01% electrodes.

Concentration-dependent enhancement of electrocatalytic H_2 production and MES performance with nickel

The concentrations of liquid and gas products, as well as gaseous CO_2 concentration, were measured over time in the reactors. No liquid products were detected during abiotic experiments. During MES experiments, acetate was the main product measured in the electrolyte, and the concentration over time is shown in Fig. 2. Acetate was detected in all reactors 11 days after inoculation, and thereafter the concentration increased until the end of the experiment. The concentration of acetate was significantly higher throughout the experiment with AC-Ni 5% electrodes, with a 25 times higher concentration by the end of the experiment (*i.e.*, over 3 g L^{-1}), compared to reactors with control electrodes (136 mg L^{-1}). Low Ni loading also led to a measurable increase of acetate production compared to control electrodes, particularly after day 21, resulting in 3.5 times higher concentration (*i.e.*, 472 mg L^{-1}) by the end of the experiment
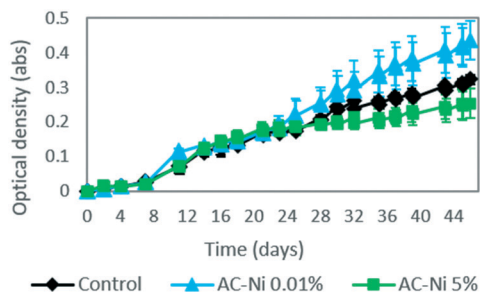
Fig. 4 Average optical density in the electrolyte over time during MES experiments. At each sampling point, both the measured and the calculated value after refreshing the electrolyte are shown. Error bars indicate the standard deviation based on duplicate experiments.

(Fig. 2). This is in line with the increased current density of AC-Ni 0.01%, compared to control AC, after day 20 (Fig. 1c), thus suggesting that higher current density was due to differences in biocatalytic, rather than electrocatalytic, activity between reactors with these two electrodes.

Aside from acetate, formate was also detected in the electrolyte during MES experiments, and the concentration over time is shown in Fig. 2. Formate, an intermediate product during acetate biosynthesis,[29] was initially formed and thereafter depleted from the electrolyte in all MES experiments. The difference in formate concentration does not appear to be significant among reactors. However, it can be observed that the peak in formate concentration was recorded earlier in reactors with AC-Ni 5% electrodes, followed by AC-Ni 0.01%, and thereafter control electrodes.

H_2 was the only product detected during abiotic experiments, and the calculated electron recovery is shown in Fig. 3a. The average electron recovery to H_2 was slightly higher with AC-Ni 0.01% compared to control electrodes, but the two values were not significantly different, based on duplicate experiments (Fig. 3a). Therefore, adding a small amount of Ni did not improve the electrocatalytic H_2 production, as was also evident by the current density (Fig. 1a). Low loading likely resulted in formation of too small and/or scarce Ni nanostructures on AC for measurable H_2 production. Instead, AC-Ni 5% had a significantly higher electron recovery into H_2 at every time point, compared to the other two electrodes, reaching a maximum electron recovery of up to 90% on day 4, and an over 6-fold increase compared to control electrodes on day 7 (Fig. 3a). For all three electrodes, the electron recovery was less than 100%, which may indicate that some H_2 was leaking out of the reactor or adsorbed on the AC electrode over time.[30]

Gas products were also measured during MES experiments, namely H_2 and CH_4. The calculated electron recovery into H_2 is shown in Fig. 3a. As was also observed during abiotic experiments, H_2 production was higher in reactors with AC-Ni 5%, whereas the difference observed between the other two AC electrodes was not significant (Fig. 3a). The highest average electron recovery was recorded on day 7 and corresponded to 76% for MES reactors with AC-Ni 5%. H_2 production could be observed until day 11 in reactors with AC-Ni 5%, with an electron recovery of over 60%, whereas it drastically dropped to 10% by day 14. Only trace amounts of H_2 could be measured from day 16 onwards. Similarly, H_2 production decreased in MES reactors with control and AC-Ni 0.01% electrodes after day 9, and only trace amounts of H_2 could be detected after day 18.

The electron recovery into CH_4 over time during MES experiments is also shown in Fig. 3a. CH_4 production was recorded in all reactors during later stages of reactor operation, which coincided with a lower apparent H_2 production. Production was detected earlier in reactors with AC-Ni 5% cathodes (day 14), followed by AC-Ni 0.01% (day 18) and thereafter control electrodes (day 23). The highest average electron recovery of over 25% was recorded with AC-Ni 5% cathodes on day 43, 29 days after the onset of production, whereas reactors with AC-Ni 0.01% and control electrodes reached a maximum of approximately 14% at the onset of production, on days 18 and 23, respectively. No CH_4 production could be detected with control and AC-Ni 0.01% electrodes after day 43, whereas production was recorded until the end of the experiment in reactors with AC-Ni 5% cathodes.

For both acetate and formate production during MES, the electron recovery was also calculated at every sampling point, and the results are shown in Fig. 3b. At almost every time point, particularly between days 14–37, the electron recovery to acetate was significantly higher in reactors with AC-Ni 5%, followed by AC-Ni 0.01% and finally control electrodes. The maximum recovery was calculated with AC-Ni 5% (74% on day 16), followed by AC-Ni 0.01% (64.5% on day 11) and control electrodes (28.5% on day 14). Instead, the highest electron recovery to formate was calculated with AC-Ni 0.01%, reaching a maximum of 20% on day 14, followed by control (12% on day 16), and last by AC-Ni 5% electrodes (2% on day 11). As an intermediate product, lower concentration and electron recovery to formate is not necessarily indicative of lower production, but could be due to the intermittent sampling and fast formate uptake by the microorganisms during MES experiments.

Enhancement of planktonic growth with low nickel loading

To visualize the growth of planktonic microorganisms, the optical density of the electrolyte was measured over time during MES experiments (Fig. 4).

For all MES reactors, the optical density increased continuously throughout the experiment. The optical density was similar among all reactors until day 25. From day 28 onwards, some deviation could be observed among experiments, with the highest optical density recorded for reactors with AC-Ni 0.01%, followed by control and finally by AC-Ni 5% electrodes. The final optical density was 35% higher with AC-Ni 0.01% electrodes, compared to control electrodes, whereas with AC-Ni 5% the final optical density was 21% lower than in reactors with control electrodes. It should be noted that optical density measurements at a single wavelength could only give a rough indication of microbial growth in mixed cultures.[31] Nevertheless, in lieu of microscopic observations in the electrolyte, the recorded differences in optical density do imply that the concentration of planktonic microorganisms was higher during experiments in reactors with AC-Ni 0.01%, followed by control and AC-Ni 5% electrodes.

Insignificant effect of nickel addition on surface properties of AC

The surface properties of the three AC samples were characterized using N_2 physisorption, and a summary of the results is shown in Table 2 (columns 2–4).

2506 | *Catal. Sci. Technol.*, 2022, **12**, 2500–2518

This journal is © The Royal Society of Chemistry 2022

Based on the standard deviation calculated for duplicate measurements, the three AC samples do not show significant differences in terms of surface properties. Aside from physisorption, AC granules were also analysed using ICP to determine the actual metal loading. Table 2 includes an overview of the metal concentration for all electrodes used (columns 5–6). As can be observed, for both Ni-impregnated electrodes, the concentration of Ni was slightly higher than the target metal loading, and corresponded to 1.7×10^{-2} % for AC-Ni 0.01% and over 6% for AC-Ni 5% (Table 2, row 3–4, column 5). This could be due to partial burning of the AC during calcination, resulting in less amount of AC and therefore higher percentage of Ni on the granules. Aside from nickel, iron was detected on all AC samples after metal extraction (Table 2, row 2–4, column 6), indicating the presence of metal impurities on the AC granules, in spite of the treatment in nitric acid that was performed before impregnation.

Effect of nickel addition on dissolved nickel concentration due to leaching and re-deposition

The concentration of dissolved Ni atoms was measured in the catholyte during the experiments, and the results are summarized in Fig. 5, for both abiotic (Fig. 5a and b) and MES (Fig. 5c–e) experiments. At the start of the experiment, electrodes were added in the reactors, and the electrolyte was flushed with CO_2 for 30 minutes. The samples corresponding to time point zero in Fig. 5 were taken at the end of this 30 minute period, before potential was controlled. Compared to

fresh electrolyte, which had a concentration of 5.7 μg L^{-1}, the concentration of dissolved Ni was higher in every reactor at time point zero during abiotic experiments, and corresponded to approximately 16 mg L^{-1} for AC-Ni 5%, 90 μg L^{-1} for AC-Ni 0.01%, and 15 μg L^{-1} for reactors with control electrodes (Fig. 5a and b). The same trend was also observed during MES experiments, with the concentration of dissolved Ni at time point zero reaching 15 mg L^{-1} for AC-Ni 5%, followed by 70 μg L^{-1} for AC-Ni 0.01% and 12 μg L^{-1} for reactors with control electrodes (Fig. 5c and e).

High concentration of dissolved Ni atoms in the electrolyte at the start of the experiment indicates that leaching occurred for both Ni oxide-impregnated electrodes. Compared to the total amount of Ni on each electrode (Table 2) and in the microbial growth medium (in Experimental section), it can be calculated that leaching corresponded to approximately 10% for AC-Ni 0.01% and 5% for AC-Ni 5% electrodes. For control electrodes, the deviation between the expected (5.7 μg L^{-1}) and the measured concentration (12–15 μg L^{-1}) of Ni cannot be attributed to leaching, and is therefore likely due to inaccuracies in the measurement, as the level of quantification for ICP performed in our laboratories is set at 10 μg L^{-1}.

For both abiotic (Fig. 5a) and MES experiments (Fig. 5c) with AC-Ni 5%, the concentration of Ni atoms in the electrolyte decreased over time until day 7 to approximately 1 mg L^{-1}, and thereafter remained somewhat more stable until the end of the experiment. Decreasing concentration over time indicates that dissolved Ni oxide was reduced and re-deposited on the electrode, due to the cathode potential
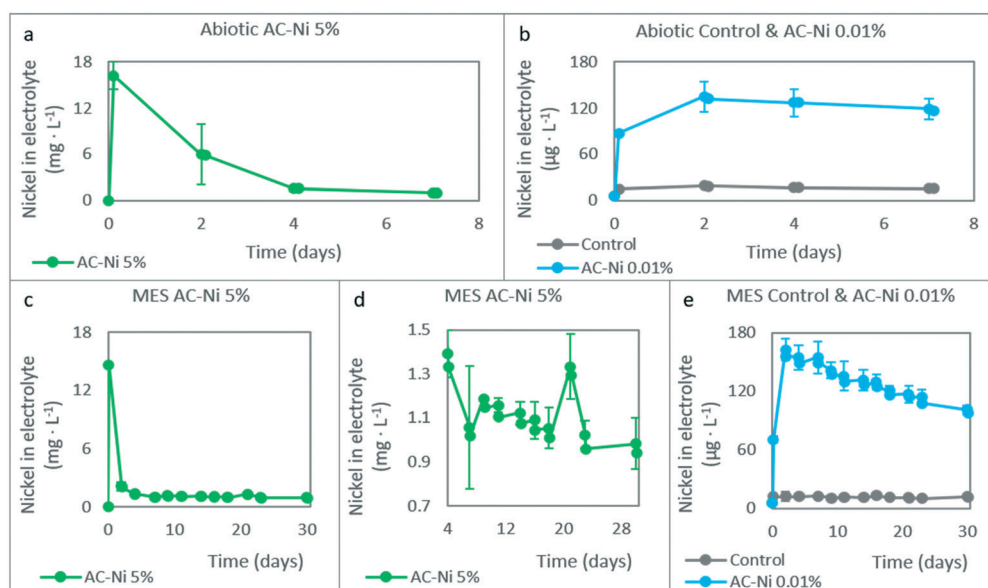
Fig. 5 Average Ni atom concentration (dissolved as nickel oxide) in the electrolyte over time during abiotic (a and b) and MES (c–e) experiments. Average values are based on duplicate experiments, and error bars indicate standard deviation. At each sampling point, both the measured and the calculated concentration after refreshing the electrolyte are shown. In figure c, data is shown between days 0–30 of MES experiments, whereas in figure d, data for reactors with AC-Ni 5% are shown between days 7–30 at a different scale, to better illustrate the decrease in concentration during this stage. For comparison, the concentration of Ni in fresh electrolyte was 5.7 μg L^{-1}. The first time point corresponds to samples taken 30 minutes after the electrodes were added in the reactor, before applying a negative cathode potential.

This journal is © The Royal Society of Chemistry 2022

Catal. Sci. Technol., 2022, 12, 2500–2518 | 2507

applied, or utilized by microorganisms, in the case of MES experiments. Unlike reactors with AC-Ni 5%, which reached the highest dissolved Ni atom concentration on day zero, reactors with AC-Ni 0.01% reached the highest concentration at the second measurement time point on day 2, which corresponded to 135 μg L^{-1} for abiotic (Fig. 5b) and 163 μg L^{-1} for MES experiments (Fig. 5e). Thereafter, the concentration decreased over time until the end of the experiment. Clearly, both leaching and re-deposition seem to have occurred at different rates in reactors with AC-Ni 0.01%, compared to AC-Ni 5%, and this was likely related to the total concentration of the metal, as all other factors among the different experiments were the same (*e.g.*, cathode potential, sampling frequency).

Unlike the experiments with Ni-impregnated electrodes, which show variations in the concentration of dissolved Ni over time due to leaching and re-deposition, the concentration in reactors with control electrodes remained stable over time, at less than 20 μg L^{-1} for both abiotic (Fig. 5b) and MES experiments (Fig. 5e). This is likely due to EDTA added in the electrolyte, a chelating agent that stabilizes dissolved metal species,[32] and prevents the depletion of the metal due to electrodeposition.[33] It should be noted that the EDTA concentration in the electrolyte was selected based on the native concentration of metals (*i.e.*, concentration given in the Experimental section), and was not adapted to stabilize the additional amount of Ni during experiments with AC-Ni electrodes. Thus, for Ni-impregnated electrodes, due to the opposing forces of EDTA and the negative cathode potential applied, the dissolved metal concentration remained relatively high throughout the experiment, *i.e.*, over 900 μg L^{-1} with AC-Ni 5%, and 100 μg L^{-1} with AC-Ni 0.01% electrodes during MES experiments (Fig. 5c–e). With both Ni-impregnated electrodes, the concentration of dissolved Ni in the electrolyte during MES experiments continued to decrease over time at a slower rate after day 7, possibly due to microbial utilization. With AC-Ni 5%, due to the much higher total concentration, this trend is not as obvious in Fig. 5c. For a clearer visualization, this time period in reactors with AC-Ni 5% electrodes during MES is shown in Fig. 5d. After correcting for dilution due to sampling and adding fresh electrolyte, the actual decrease in concentration between days 7–30 corresponded to 29 μg L^{-1} with AC-Ni 0.01%, whereas the concentration increased in the electrolytes with AC-Ni 5% electrodes by 150 μg L^{-1}, likely due to leaching from the electrode during OCP around day 20.

Microbial utilization of dissolved nickel and formation of nickel structures for improved biofilm formation

Electrodes were characterized before and after MES experiments with SEM-EDX, and characteristic pictures are shown for each type in Fig. 6 and 7. Aside from microscopic, visual comparison of the biofilm-covered granules was used to compare the electrodes, and photographs of dry granules are shown in Fig. 7d.
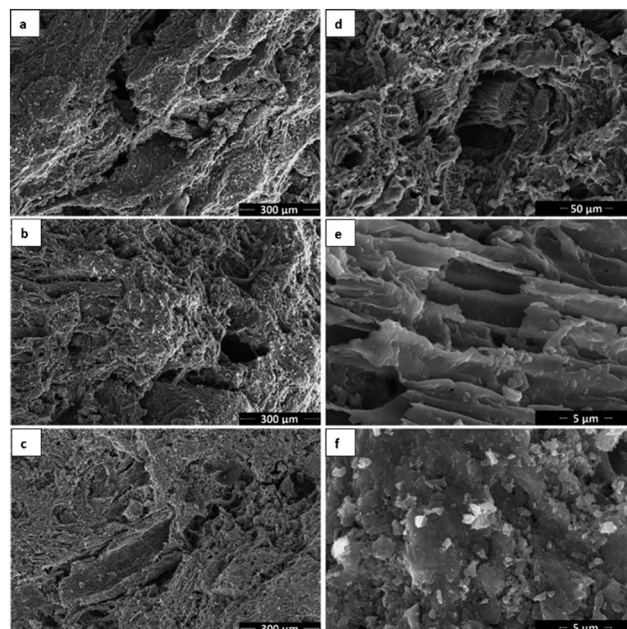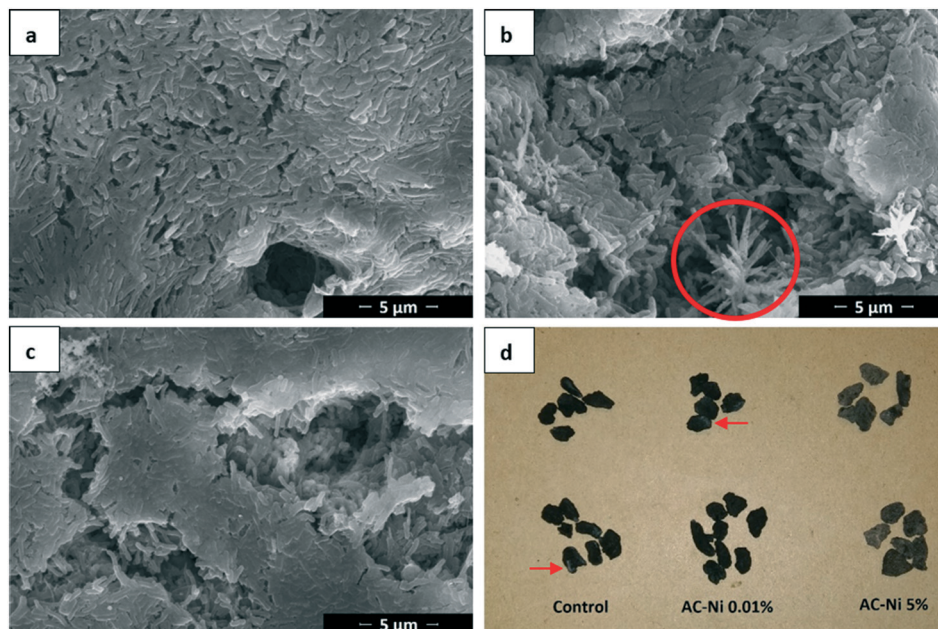

Fig. 6 SEM at various magnifications of unused granules from control AC (a), AC-Ni 0.01% (b, d and e) and AC-Ni 5% samples (c and f). On all three samples, hollow tubular structures (d and e), as well as amorphous areas (f) can be observed.

Fig. 6 shows unused AC granules at various magnifications without metal (a), with 0.01% Ni (b, d and e) and 5% Ni (c and f). No differences could be observed in the microscopic structure of the different electrode types. The surface of the granules was heterogeneous, including rather amorphous areas (d and f), as well as areas with characteristic tubular structure (d) and channels (e), likely as residues of natural structures in the plant precursor of the AC.[34] Ni could be detected on both AC-Ni electrodes with EDX, but no Ni structures could be distinguished at a magnification of up to 35 000 with SEM. For better visualization of Ni nanostructures, samples were also analysed with transmission electron microscopy, and characteristic images are shown in Fig. S1 (in ESI†).

Fig. 7 shows characteristic SEM images after MES operation of all three electrodes. As can be observed, a uniform layer of biofilm was formed on all electrodes, consisting of rod-shaped microorganisms that form an extensive network on the electrode. Filamentous structures can also be observed among the cells.

The amount of biofilm could not be compared among samples based on electron microscopy observation, as all samples exhibited full coverage with high biofilm density, consisting of multiple layers. Instead, visual observation of the three biofilm-covered AC samples was performed, and a characteristic image is shown in Fig. 7d. White coloured precipitates can be observed on all samples, highlighted with red arrows for control and AC-Ni 0.01% samples in the figure. Similar structures always appear on electrodes after MES testing, whereas they are not formed during abiotic experiments, and are therefore attributed to biofilm

2508 | *Catal. Sci. Technol.*, 2022, **12**, 2500–2518

This journal is © The Royal Society of Chemistry 2022

Fig. 7 SEM images for control AC (a), AC-Ni 0.01% (b) and AC-Ni 5% (c) electrodes, and photograph (d) of dried granules after MES experiments (with sample from each of the duplicate reactors shown in the top and bottom part of the photograph). Crystal formation was observed on AC-Ni 0.01% (b) and 5% electrodes (not shown) after MES, and characteristic crystals are highlighted with a red circle (b). White coloured precipitate on control and AC-Ni 0.01% granules are indicated with red arrows, whereas AC-Ni 5% granules are completely covered by these precipitates, resulting in an apparent grey colour of the granules (d).

formation. As can be observed, white structures were only visible on some parts of the control and low Ni loading electrodes. Instead, AC-Ni 5% granules were completely covered by these structures, resulting in an apparent grey
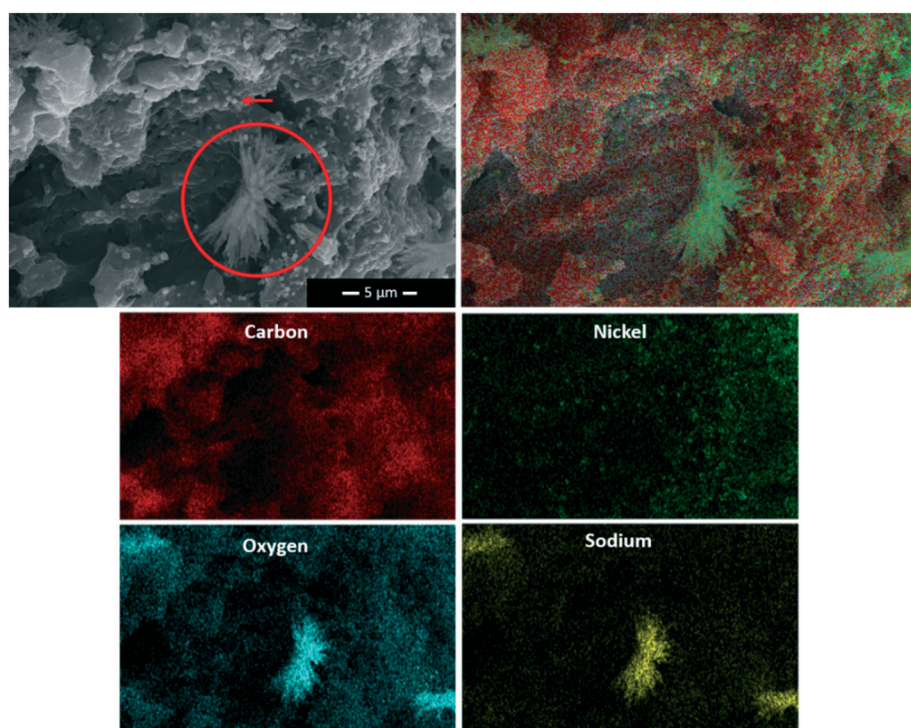
Fig. 8 SEM-EDX analysis on AC-Ni 5% granules after MES operation. Dendrite crystals (highlighted with red circle) can be observed on the cathode (green colour in layered map image), consisting of Na (yellow) and O (blue). In addition, large particles (indicated with red arrow) can be observed on top of the biofilm (green spots in layered map image), which consist of Ni (green).

colour of these granules, compared to the black colour of the other two samples. This observation suggest that more or thicker biofilm was formed on the AC-Ni 5% electrode. Furthermore, this observation confirms that microorganisms could access the external surface area of all the granules on the electrode, despite the confinement in the polypropylene tube.

Dendrite crystals could also be observed with SEM on the two AC-Ni electrodes, as can be seen for example for AC-Ni 0.01% in Fig. 7b (highlighted with red circle). To further investigate these structures, SEM-EDX was performed, and a characteristic image is shown in Fig. 8 (crystal highlighted with red circle), accompanied by maps for individual elements detected on the sample. The composition of the crystals was mainly Na and O, indicating sodium hydroxide crystals. On control electrodes, amorphous rather than crystalline deposits could be observed that had the same composition (not shown in Fig. 7a). Amorphous or crystalline solid artefact formation has been previously reported during SEM sample preparation.[35,36] Alternatively, crystallization may have occurred during cathodic operation (at −1.06 V *vs.* Ag/AgCl and pH of approximately 6.7).

EDX on the AC-Ni 5% electrode after MES operation revealed large particles that consist of Ni on top of the biofilm surface (indicated with red arrow in Fig. 8). Based on ICP measurements in the electrolyte (Fig. 5), re-deposition of the leached Ni occurred primarily during the first four days of both abiotic and MES experiments, whereas biofilm growth likely occurred throughout the experiment.[37] Thus, if these large Ni particles were formed due to electrodeposition, they would be on the activated carbon and the initial layer of biofilm resulting from the inoculum, with more biofilm growing on top of them over time until the end of the experiment. The fact that the Ni particles are on the outermost surface of the biofilm implies that these are bio-crystallised structures, using H_2 or electrons from the electrode as an electron donor for the reduction of dissolved Ni. Alternatively, they may be formed during the SEM sample preparation. While Ni is an essential element for microbial growth in trace amounts, it has been shown to inhibit microbial activity with increasing amounts, with concentrations as low as 1 mg L^{-1} being inhibiting in certain studies.[38] Throughout MES experiments with AC-Ni 5% electrodes, the Ni atom concentration in the electrolyte was higher or equal to 1 mg L^{-1} (Fig. 5b). Bio-crystalized Ni structures on the electrode could therefore be a response of microorganisms to inhibiting concentrations of the dissolved metal, as a mechanism to decrease the potential toxic effects of high Ni concentration in the electrolyte.

Concentration-dependent effect of nickel on planktonic microbial community composition

The microbial community composition was analysed for each reactor at the end of MES experiments. Aside from the experimental reactors, the inoculum used at the start of the experiment was also analysed. An overview of the relative abundance of different families in each reactor and in the inoculum is shown in Fig. S2 (in ESI†). In terms of average distribution within all the samples, the dominant phylum (>10% relative abundance) was *Proteobacteria* (63.3 ± 25.9%), followed by *Firmicutes* (24.7 ± 18.6%). The majority of the microorganisms identified were bacteria, whereas some unidentified operational taxonomic units (OTUs) (about 0.5% in all samples) and methanogenic archaea (*Euryarchaeota*) were also present, primarily in the inoculum sample (19.6%). Interestingly, nearly 1% of *Methanobrevibacter* were present in reactors with AC-Ni 5%, despite the addition of the methanogen inhibitor $BrCH_2CH_2SO_3Na$. Previous MES studies have also reported the presence of methanogens, despite addition of this compound.[2] It has been shown that the methanogen inhibitor in the catholyte mainly inhibits methanogenic species on the electrode, whereas they can still be abundant in the electrolyte, due to the adsorption of the inhibitor on the carbonaceous electrode.[39] The most dominant families among all the samples were *Helicobacteraceae* (42.6 ± 18.7%), *Peptococcaceae* (11.6 ± 16.9%), *Veillonellaceae* (11 ± 4.2%) and *Desulfovibrionaceae* (10.6 ± 4%). The most dominant genera identified are presented in Fig. 9, whereas genera with a smaller contribution are shown in Fig. S3 and S4 (in ESI†).

Among the three experimental reactors and the parent reactor, significant differences can be observed in terms of microbial community composition at all taxonomic levels. Some OTUs have a much higher abundance in the inoculum, compared to experimental reactors, such as the family *Ruminococcaceae* (primarily genus *Oscillibacter*), *Porphyromonadaceae* and *Lentimicrobiaceae*. This is likely due to the metabolic and symbiotic role of these taxa. *Ruminococcaceae* are known to metabolize a variety of complex polysaccharides,[40–43] and may be therefore more abundant in the parent reactor, due to the availability of more complex substrates. Similarly, members of the family of *Porphyromonadaceae*, characterized by a proteolytic metabolism,[44] likely grow symbiotically with other microbes in the parent reactor, and consume organic matter released in the electrolyte from the decay of other bacteria. Unclassified *Lentimicrobiaceae* species have been recently identified as potential acetate-oxidizing bacteria in thermophilic methanogenic chemostats,[45] and their higher abundance in the parent reactor may be related to the higher acetate concentration. On the contrary, the family of *Comamonadaceae* (primarily genus *Hydrogenophaga*) exhibited higher abundance of over 8% in experimental reactors, compared to the parent reactor (<2%). Several metabolic pathways have been described for strains in this genus, including CO_2 fixation using H_2.[46] Therefore, higher abundance in experimental reactors may be due to H_2 accumulation, whereas in the parent reactor gas products were allowed to escape *via* a water-lock.

Among the taxonomic units that exhibited high abundance in experimental reactors, different trends were
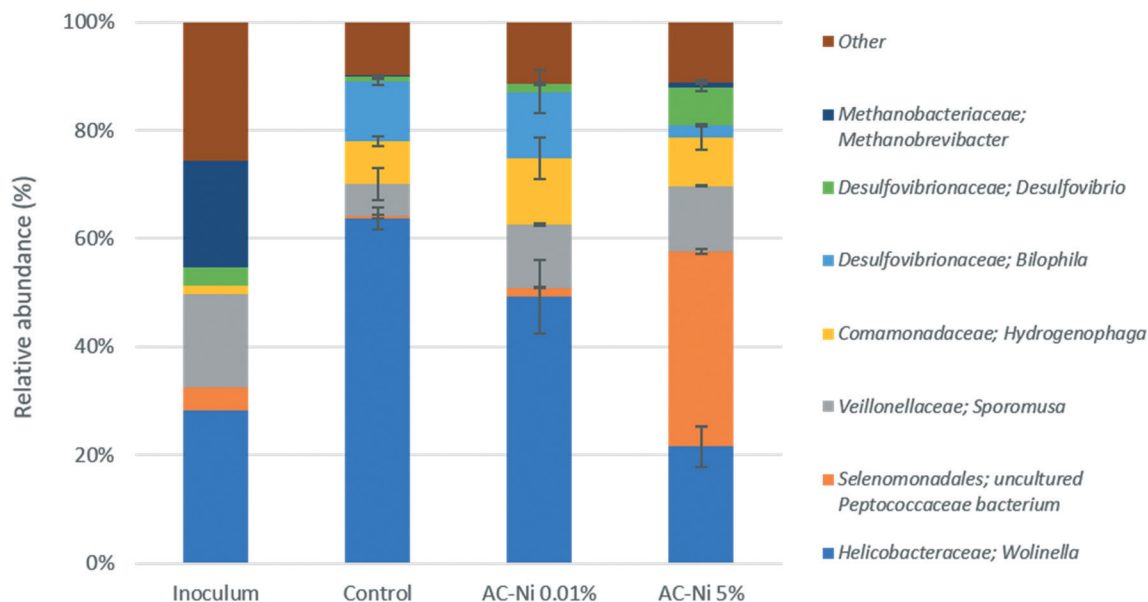
2510 | *Catal. Sci. Technol.*, 2022, **12**, 2500–2518

This journal is © The Royal Society of Chemistry 2022

Fig. 9 Main genera identified in the inoculum and in experimental reactors. Inoculum sample was not analysed in duplicate. For MES reactors, the average values given are based on duplicate reactors, and error bars indicate the standard deviation between duplicates.

observed, depending on the Ni loading. For example, *Helicobacteraceae* (primarily genus *Wolinella*) exhibited a higher abundance of up to 64% in reactors with control and AC-Ni 0.01% electrodes, compared to AC-Ni 5% (22%) and parent (28.5%) reactors. A similar trend can be observed for the family *Desulfovibrionaceae* (primarily the genus *Bilophila*), with up to 14% abundance in reactors with control and AC-Ni 0.01% electrodes, compared to AC-Ni 5% (9%) and parent (3%) reactors. On the contrary, *Peptococcaceae* exhibited the highest abundance in reactors with AC-Ni 5% electrodes (over 36%) whereas less than 2% was found in the other two reactors. While all three families include H_2-consuming strains,[47–49] the different trends in microbial composition may be related to other factors, such as Ni concentration and competition with other taxa, as will be further explained in the Discussion section. It should be noted that the reactors were operated in batch mode, and microbial community composition was not analysed over time, but only at the end of the experiment. Therefore, some OTUs detected may not have been metabolically active or dominant throughout the experiment, but due to lack of complete renewal of the electrolyte, they did not get washed out, and can still be detected during community composition analysis.

Discussion

Among the potential mechanisms of interaction between Ni and MES, presented in Table 1, some could not be investigated in the present study, whereas others were shown to have an insignificant effect on MES performance. More specifically, among the electrode properties that could affect MES, the charge transfer resistance, electrode conductivity and availability of redox mediators were omitted, and will

therefore not be further discussed here. Ni impregnation resulted in an insignificant effect on electrode properties, such as surface area and pore structure. On the contrary, Ni addition on AC was shown to significantly affect the electrocatalytic production of electron donors at high metal loadings (*i.e.*, H_2), as well as the availability of dissolved Ni ions at both metal loadings, which has a role as a trace element, but can also be toxic for microorganisms at high concentrations. Finally, aside from the mechanisms presented in Table 1, the presence of large Ni particles within the biofilm at the end of MES experiments revealed another possible mechanism of interaction between dissolved Ni and MES, as a source of Ni for the formation of bio-crystalized structures.

In order to determine the factors that affect the MES performance and microbial community composition, the Spearman's correlation coefficient was calculated for the main genera identified in experimental reactors and several parameters measured during MES experiments (Table 3). As can be observed, there are numerous significant correlations among experimental parameters and the relative abundance of certain OTUs, such as between abiotic H_2 production and the family of *Peptococcaceae*, which exhibits a positive correlation with two-star significance. Some negative correlations can also be observed, such as between *Azonexus* and dissolved Ni concentration. Certain correlations can also be observed between experimental parameters, such as between the onset of acetate production and the abiotic H_2 production, which implies that acetate production begins earlier in reactors with higher abiotic H_2 production. Finally, correlations can also be observed among the different OTUs, which can be positive (such as between *Wolinella* and *Azonexus*), thus indicating a symbiotic effect, or negative

This journal is © The Royal Society of Chemistry 2022

Catal. Sci. Technol., 2022, **12**, 2500–2518 | **2511**

Table 3 Spearman's correlation coefficient calculated for several experimental parameters and the relative abundance of the most dominant OTUs at the genus level. Abiotic and MES H_2 production refer to the electron recovery calculated on day 7 during abiotic and MES experiments, respectively. This time point was selected, as it was indicative of long-term operation during abiotic experiments (which only lasted 7 days). MES CH_4 production corresponds to the calculated electron recovery on day 43, as methanogenic activity was well established in all reactors by this point. MES acetate production refers to the concentration of acetate in the electrolyte on day 46 (*i.e.*, end of the experiment). As acetate accumulated in the reactors over time, the final concentration was selected as it was indicative of the total production in each reactor. With the same logic, the cumulative charge and the OD values used in this test also correspond to day 46. Formate and acetate onset refer to the day that production of this compounds begun, *i.e.*, that a measurable concentration was detected in the electrolyte. Dissolved Ni oxide concentration values correspond to day 30, which was the last measuring point during MES experiments. *Correlation is significant at the 0.05 level (2-tailed). **Correlation is significant at the 0.01 level (2-tailed)

	Abiotic H$_2$	Formate onset	Acetate onset	OD	Dissolved Ni	MES H$_2$	MES CH$_4$	MES acetate	Charge	*Wolinella*	*Peptococcaceae*	*Sporomusa*	*Hydrogenophaga*	*Bilophila*	*Desulfovibrio*	*Methanobrevibacter*	*Lentimicrobium*	*Azonexus*	*Kerstersia*
Abiotic H$_2$	1.000	−0.794	**−0.926****	−0.543	0.829*	0.543	0.600	0.771	−0.886*	−0.714	**0.943****	0.657	0.029	−0.771	0.714	0.600	0.543	−0.714	−0.600
Formate onset	−0.794	1.000	**0.953****	0.618	−0.794	−0.883*	−0.530	**−0.971****	0.883*	0.883*	−0.883*	−0.883*	−0.265	0.530	−0.883*	−0.794	−0.794	0.883*	0.618
Acetate onset	**−0.926****	**0.953****	1.000	0.679	−0.802	−0.802	−0.555	**−0.926****	**0.926****	0.802	**−0.926****	−0.802	−0.062	0.679	−0.802	−0.802	−0.679	0.802	0.679
OD	−0.543	0.618	0.679	1.000	−0.371	−0.829*	−0.543	−0.543	0.486	0.429	−0.429	−0.486	0.429	0.600	−0.429	**−0.943****	−0.543	0.429	**0.943****
Dissolved Ni	0.829*	−0.794	−0.802	−0.371	1.000	0.543	0.829*	0.829*	−0.886*	**−0.943****	**0.943****	0.886*	0.429	−0.771	**0.943****	0.429	0.829*	**−0.943****	−0.429
MES H$_2$	0.543	−0.883*	−0.802	−0.829*	0.543	1.000	0.486	0.829*	−0.657	−0.714	0.600	0.771	0.029	−0.429	0.714	**0.943****	0.771	−0.714	−0.771
MES CH$_4$	0.600	−0.530	−0.555	−0.543	0.829*	0.486	1.000	0.543	−0.600	−0.771	0.657	0.714	0.200	−0.829*	0.771	0.429	0.829*	−0.771	−0.600
MES acetate	0.771	**−0.971****	**−0.926****	−0.543	0.829*	0.829*	0.543	1.000	**−0.943****	−0.886*	0.886*	**0.943****	0.257	−0.600	0.886*	0.714	0.771	−0.886*	−0.486
Charge	−0.886*	0.883*	**0.926****	0.486	−0.886*	−0.657	−0.600	**−0.943****	1.000	0.829*	**−0.943****	−0.886*	−0.143	0.771	−0.829*	−0.600	−0.657	0.829*	0.429
Wolinella	−0.714	0.883*	0.802	0.429	**−0.943****	−0.714	−0.771	−0.886*	0.829*	1.000	−0.886*	**−0.943****	−0.543	0.600	**−1.000****	−0.543	**−0.943****	**1.000****	0.486
Peptococcaceae	**0.943****	−0.883*	**−0.926****	−0.429	**0.943****	0.600	0.657	0.886*	**−0.943****	−0.886*	1.000	0.829*	0.314	−0.714	0.886*	0.543	0.714	−0.886*	−0.486
Sporomusa	0.657	−0.883*	−0.802	−0.486	0.886*	0.771	0.714	**0.943****	−0.886*	**−0.943****	0.829*	1.000	0.371	−0.657	**0.943****	0.600	0.886*	**−0.943****	−0.429
Hydrogenophaga	0.029	−0.265	−0.062	0.429	0.429	0.029	0.200	0.257	−0.143	−0.543	0.314	0.371	1.000	0.200	0.543	−0.257	0.486	−0.543	0.257
Bilophila	−0.771	0.530	0.679	0.600	−0.771	−0.429	−0.829*	−0.600	0.771	0.600	−0.714	−0.657	0.200	1.000	−0.600	−0.486	−0.543	0.600	0.543
Desulfovibrio	0.714	−0.883*	−0.802	−0.429	**0.943****	0.714	0.771	0.886*	−0.829*	**−1.000****	0.886*	**0.943****	0.543	−0.600	1.000	0.543	**0.943****	**−1.000****	−0.486
Methanobrevibacter	0.600	−0.794	−0.802	**−0.943****	0.429	**0.943****	0.429	0.714	−0.600	−0.543	0.543	0.600	−0.257	−0.486	0.543	1.000	0.600	−0.543	−0.886*
Lentimicrobium	0.543	−0.794	−0.679	−0.543	0.829*	0.771	0.829*	0.771	−0.657	**−0.943****	0.714	0.886*	0.486	−0.543	**0.943****	0.600	1.000	**−0.943****	−0.600
Azonexus	−0.714	0.883*	0.802	0.429	**−0.943****	−0.714	−0.771	−0.886*	0.829*	**1.000****	−0.886*	**−0.943****	−0.543	0.600	**−1.000****	−0.543	**−0.943****	1.000	0.486
Kerstersia	−0.600	0.618	0.679	**0.943****	−0.429	−0.771	−0.600	−0.486	0.429	0.486	−0.486	−0.429	0.257	0.543	−0.486	−0.886*	−0.600	0.486	1.000

(such as between *Azonexus* and *Desulfovibrio*), which implies competition between these two OTUs.

Concentration-dependent effect of nickel on microbial growth reveals the role of nickel as toxic compound, electrocatalyst, conductive material and trace element

Decreased planktonic growth and increased biofilm formation with AC-Ni 5% as a result of nickel toxicity. An improvement in microbial growth of planktonic microorganisms was expected with AC-Ni 5%, due to the superior catalytic activity of this electrode for H_2 production (Fig. 3), which can serve as an electron mediator for planktonic microorganisms. Previous studies on biocathode modification with molybdenum electrocatalysts have also shown the beneficial effect of metal modification on the growth of planktonic microorganisms, likely due to improved H_2 production by the metal catalyst, using carbon felt electrodes operating at −0.85 V *vs.* SHE at a current density of approximately −0.4 mA–cm^{-3}.[8] Instead, the low optical density recorded in reactors with AC-Ni 5% electrodes here implied that H_2 production did not give a competitive advantage to planktonic microorganisms, compared to the other two electrodes. Low optical density in the presence of AC-Ni 5% electrode was possibly due to the inhibiting effect of high dissolved Ni concentration (Fig. 5) on MES microorganisms. In fact, high dissolved Ni concentration in the catholyte may further explain the improved biofilm formation on AC-Ni 5% electrodes, compared to the other two electrode types. It has been previously shown that biofilm formation can be used as a response of bacteria to stressful conditions, such as high Ni concentration, and this response is regulated *via* a transcriptional effect on genes responsible for biofilm formation.[50] Upon exposure to nickel and copper surfaces, studies on gene expression have revealed the upregulation of genes related to general stress response,

2512 | *Catal. Sci. Technol.*, 2022, **12**, 2500–2518

This journal is © The Royal Society of Chemistry 2022

colony morphology, auto-aggregation ability control and metal-binding proteins.[51] While differences in colony morphology and gene expression were not investigated in the present study, it is possible that improved biofilm formation and decreased planktonic growth in reactors with AC-Ni 5% electrodes was a response to high Ni concentration. Ni structures observed with SEM-EDX on the outermost layer of biofilm on AC-Ni 5% electrodes (Fig. 8) could further support the toxic effects of Ni, as bio-crystallization may have been used by microorganisms to decrease toxic dissolved Ni concentrations. Nevertheless, no significant correlation between optical density and dissolved Ni concentration could be observed based on the statistical analysis performed (Table 3), and thus this mechanism of interaction between Ni and MES microorganisms cannot be further substantiated.

The potentially inhibiting effects of high dissolved Ni concentration are also evident based on the microbial community composition. For example, the order of *Selenomonadales* (unclassified *Peptococcaceae* bacterium) had highest abundance in reactors with AC-Ni 5% electrodes (36%), followed by inoculum (4.1%), AC-Ni 0.01% (1.8%) and control samples (0.4%), which could be due to their tolerance to high dissolved Ni concentration, compared to other groups, as sulfate-reducing bacteria including *Peptococcaceae* are often found in metal-rich sites.[52–54] This hypothesis is further substantiated by the statistical analysis performed, which shows a strong positive correlation between the abundance of *Peptococcaceae* and the dissolved Ni concentration (Table 3).

Another strong positive correlation with dissolved Ni concentration was calculated for *Desulfovibrio* (Table 3), which exhibited highest abundance in the reactors with AC-Ni 5% electrodes (7.1%), followed by the inoculum (3.4%), AC-Ni 0.01% (1.5%) and control samples (1.1%). It has been previously shown that the abundance of *Desulfovibrio* in mixed cultures increases with increasing copper amounts on steel supports.[55] Increased abundance with increasing copper amounts may be linked to the corrosion acceleration mechanisms employed by *Desulfovibrio* and other sulfate-reducing bacteria, including direct biocatalytic cathodic electron transfer.[55] Thus, a similar mechanism to copper tolerance can be hypothesized for Ni, which could explain the higher abundance of *Desulfovibrio* with AC-Ni 5% electrodes.

Biofilm enhancement, syntrophy and competition based on H_2 as an electron donor. While the increased H_2 production with AC-Ni 5% was not shown to improve the growth of planktonic microorganisms, it could explain the higher biofilm coverage on AC-Ni 5%, compared to the other two electrodes. Previous studies on biocathode modification with H_2-producing electrocatalysts have also correlated the improved biofilm formation on the modified electrodes to improved H_2 production, compared to control electrodes.[8] In fact, effective scavenging of the electrocatalytically produced H_2 by biofilm-forming microorganisms, which are in close proximity to the electrode, as has been previously shown,[2,10] could further explain the lower growth of planktonic

microorganisms in this reactor, as H_2 may have been consumed before it could be dissolved in the electrolyte, and thus limit the availability of electron donors for planktonic microorganisms. Effective scavenging of H_2 by biofilm-forming microorganisms may further explain the lack of H_2 detected with GC after day 11 (Fig. 3). H_2 consumption within the biofilm contradicts our findings of strong correlation between the electrocatalytic H_2 production and the abundance of certain OTUs with a known hydrogenotrophic metabolism in the planktonic phase, such as unclassified *Peptococcaceae* bacterium,[49] and hydrogenotrophic methanogenic archaea.[56] This could imply that H_2 is not fully depleted within the biofilm, but part of the electrocatalytically produced H_2 is dissolved in the electrolyte, and thereafter depleted by planktonic microorganisms. Alternatively, it could be hypothesized that these OTUs originate from the biofilm, and were detached. The high abundance of these OTUs in the planktonic phase could also be due to syntrophic effects with H_2-producing microorganisms detected in the present study. For example, the co-occurrence between hydrogenotrophic methanogens (including *Methanobrevibacter)* and fermenting bacteria (*e.g.*, *Bacteroidetes*, *Spirochaetes*) has been previously reported in anaerobic digestion reactors, as the latter are capable of hydrolysis and produce intermediates, *e.g.*, H_2/CO_2, formate, and acetate.[57] Acetate oxidizing bacteria within the phylum *Synergistetes* and the family *Lentimicrobiaceae* may have also operated in symbiosis with hydrogenophilic methanogens, as has been previously shown.[45,58] A syntrophic effect based on H_2 is also evident between *Wolinella* and *Sporomusa*, which can both consume H_2 to reduce nitrate, sulfur and fumarate[59–61] or CO_2,[62] respectively. The strong negative correlation between these OTUs (Table 3) likely indicates competition for H_2.

Consumption of H_2 near the surface of the electrode by biofilm-forming microorganisms in the present study complicates the interpretation of the interaction between planktonic growth/community composition and electrocatalytic activity of the modified electrodes for H_2 production. Therefore, while AC is clearly a suitable electrode material for MES, future studies on electrocatalytic cooperation based on H_2 intermediate would likely benefit from the use of a less biocompatible electrode with strong H_2 evolution activity, such as a pure metallic nickel foil or mesh. Alternatively, the effect of H_2 as an electron donor could also be investigated under different cathode potentials, in order to tune the H_2 production, or *via* feeding electrochemical reactors with specific H_2/CO_2 ratios.

Improved conductivity within the biofilm *via* bio-crystallization of dissolved nickel. By the end of the experiment, Ni structures could be detected on the biofilm with AC-Ni 5%, whereas these were not observed with the other two electrode types (Fig. 8). A previous bio-electrochemical study with pure cultures of *Desulfovibrio desulfuricans* on bioanodes has revealed the ability of the microbe to form Pd nanoparticles from dissolved Pd ions in solution, which can be found on the

This journal is © The Royal Society of Chemistry 2022

Catal. Sci. Technol., 2022, **12**, 2500–2518 | **2513**

extracellular surface of the microbes, and have been shown to improve the electron transfer between the microorganisms and the electrode.[63] Pd nanoparticles present on the membrane, alongside the enzymes responsible for electron transfer (cytochromes, hydrogenases), could facilitate electron transfer, due to their higher conductivity than these proteins. Thus, Pd nanoparticles possibly participate in the metabolism as biologically-derived electron carriers.[63] Aside from Pd, sulfate-reducing bacteria have also been previously shown to convert Ni from its dissolved form into nanoparticles.[64] A similar role of improving electron transfer has also been previously highlighted for iron nanostructures. For example, Li and co-workers investigated the addition of Fe_3O_4 on methanogenic microorganisms, and report that iron structures could be found attached on the surface of microbial cells, thus bridging the cell-to-cell connections for improved electron transfer.[65] In fact, some OTUs such as *Geobacteriaceae* were shown to strictly rely on the addition of iron nanostructures and their electrical conductivity. Insulating the Fe_3O_4 nanostructures or replacing them with known soluble electron shuttles negated the observed results, thus further supporting that the increased rate of methane production was due to the improved electrical conductivity for cell-to-cell electron transfer.[65] The Ni structures observed on the biofilm in the present study could have a similar role in improving conductivity within the biofilm. While the structures can only be visualized on the outermost layer of the thick biofilm with SEM-EDX, it is possible that similar structures were present throughout the biofilm thickness, thus increasing the overall electron transfer from the innermost to the outermost layer of biofilm. A similar effect has been previously shown for anodic biofilms, wherein magnetite nanostructures dispersed within the biofilm increased the electron transfer.[66] Such conductive bio-crystalized structures could therefore explain the improved biofilm formation on AC-Ni 5%, by improving the electron transfer during MES experiments, and thus offering a competitive advantage to biofilm-forming, compared to planktonic microorganisms.

Increased planktonic growth with AC-Ni 0.01% as a result of trace element availability. Reactors with AC-Ni 0.01% electrodes exhibited the highest growth of planktonic microorganisms. While some improvement in electrocatalytic H_2 production can be observed between AC-Ni 0.01% and control electrodes (Fig. 3a), the high standard deviation among duplicate control reactors reveals that this difference was not significant. Instead, in terms of optical density, as well as acetate production, AC-Ni 0.01% resulted in a clearly superior performance, compared to control electrodes. Therefore, improvement of microbial growth in the planktonic phase with AC-Ni 0.01% is not related to the electrocatalytic activity, but is possibly caused by the different concentration of dissolved Ni. Considering that dissolved Ni was not depleted over time during MES experiments with control electrodes (Fig. 5e), it appears that Ni concentration as a trace element was not limiting for microbial growth in any of the MES reactors. However, chelating agents have been

shown to inhibit the uptake of trace Ni from the medium.[67] Therefore, while trace element limitation was not evident based on the dissolved metal concentration during control experiments, the uptake of Ni by microorganisms may have been in fact inhibited due to EDTA. Higher dissolved Ni concentration in reactors with AC-Ni 0.01% may have improved the Ni uptake kinetics by microorganisms, thus leading to higher optical density in these reactors. Nevertheless, as the kinetics of Ni uptake were not evaluated for the microorganisms present in the reactors, particularly considering that a mixed culture with variable uptake kinetics was used, no conclusions can be drawn at this stage regarding the role of added Ni as a trace element and the enhancement of microbial growth. Furthermore, the simultaneous electrodeposition (due to the negative cathode potential), solubilization (due to EDTA) and microbial consumption of Ni during MES further complicate the understanding of the role of Ni as a trace element. Instead, future studies should separately examine these mechanisms, in an attempt to optimise trace element concentrations in MES systems.

For both planktonic and biofilm-forming microorganisms, altered trace metal concentration could result in different gene expression and enzymatic activities within the mixed culture.[38,67] While these effects were not investigated in the present study, it is plausible that the improved production rate and yield of acetate as a response to Ni addition was due to the effect of the added metal on gene regulation and altered activity of enzymes.

Overall, the present results indicate that nickel addition at low concentrations improves microbial planktonic growth, whereas at high concentrations, nickel results in a switch from planktonic to biofilm growth, as a result of nickel toxicity. In order to further elucidate the concentration-dependent effects of nickel, future studies should focus on a wider range of nickel loadings, including both intermediate loadings (between 0.1% and 5%), as well as loadings greater than 5%. Such investigations may help reveal an optimal nickel loading to steer biocatalysts towards planktonic or biofilm growth.

Improved product formation with added nickel reveals the role of altered microbial community composition and enhanced electron transfer

Modification of bio-electrodes with Ni has been shown to decrease resistivity and activation energy threshold of electron transfer from electrodes to bacteria, both for cathodic and anodic processes.[68–71] Previous studies on biocathode modification with metals (nickel, palladium, gold and molybdenum) have revealed a positive effect of metal addition on current density, acetate production and biofilm growth, without significantly affecting the electron recovery to acetate.[5,7,8] The observed effects have been correlated to the surface properties and electrocatalytic activity for H_2 production of the modified electrodes. In contrast to these

2514 | *Catal. Sci. Technol.*, 2022, **12**, 2500–2518

This journal is © The Royal Society of Chemistry 2022

result, modification of the AC electrode with Ni in the present study did not only result in higher production rate of acetate, but also in increased electron recovery, compared to the control AC electrode, as can be observed for both AC-Ni 0.01% and AC-Ni 5% (Fig. 3b). Therefore, additional factors should be considered to fully explain the effect of Ni addition on acetate production observed in the present study.

Improved acetate formation with nickel as a result of altered microbial community composition. One explanation for the improved product formation reported here, which was not investigated during previous studies on Ni addition on single-culture MES biocathodes,[5,7] could be enrichment of acetogenic microorganisms due to Ni impregnation of the cathodes. For example, the abundance of *Sporomusa* and *Peptococcaceae*, which can both have an acetogenic metabolism,[49,62,72,73] was found to be positively correlated to both dissolved Ni concentration and acetate production (Table 3). Therefore, higher electron recovery to acetate in Ni-containing reactors could be due to the higher abundance of these OTUs, compared to control MES reactors. Changes in microbial community composition within mixed cultures have also been previously shown as a response to the addition of conductive materials, including both metals[65,74–77] and carbonaceous materials,[78–80] and have been correlated to altered community metabolism and increased production of methane. More specifically, within the field of MES for CO_2 conversion, Tian and co-workers modified a carbonaceous biocathode electrode with a H_2-producing metal electrocatalyst, and report a decrease in the abundance within the biofilm of the electrotrophic *Arcobacter*, and an increase in the abundance of the hydrogenotrophic acetogen *Acetobacterium*, as a response to the addition of the metal catalyst.[8] Metal addition on a biocathode can alter the microbial community composition not only due to electrocatalytic effects (and thus substrate availability), but also due to enrichment of metal-reducing species. For example, Zhu and co-workers have also reported a concentration-dependent effect on MES upon metal (iron) oxide impregnation on activated carbon biocathodes.[6] Specifically, acetate production and electron recovery were shown to increase with increasing amounts of Fe_3O_4, compared to control electrodes, reaching a maximum when 38% Fe_3O_4 was added, whereas a decrease in electron recovery and acetate production was recorded when 50% Fe_3O_4 was added on the electrode. Similarly, the microbial community composition revealed a concentration-dependent effect of Fe_3O_4 addition, with *Arcobacter* and *Acetobacterium* exhibiting the highest abundance in the presence of 38% Fe_3O_4, and this was correlated to improved acetate production by the authors.[6] Overall, based on these previous reports, it can be hypothesized that Ni addition affected product formation during MES in the present study, resulting from changes in the microbial community composition, either due to the electrocatalytic activity, or the availability of Ni as an electron transfer mediator.

Improved acetate formation with nickel as a result of increased electrode and biofilm conductivity. Improved electron transfer due to added conductive nanostructures may have provided a metabolic advantage to microorganisms in reactors with AC-Ni 5%, compared to the other two electrode types. Several studies have previously exhibited a switch from H_2-based to direct electron transfer in mixed microbial communities upon addition of conductive structures.[77,79–81] This may offer an advantage, as direct electron transfer among species is considered to consume less energy, compared to the production and oxidation of H_2.[76] In the presence of conductive materials, microbial cells likely do not need to spend energy for the production of electron-shuttling biological structures, such as membrane bound pili and cytochromes, as they can rely on the added conductive structures to facilitate electron transfer.[79,81] In fact, a previous study using microbial mutants upon gene deletion further supports that biologically-formed conductive structures such as pili and cytochromes are not necessary for electron transfer in the presence of conductive materials.[82] Therefore, higher rates of acetate production observed for reactors with AC-Ni 5% electrodes in the present study may be related to the improved electron transfer, which allows microorganisms to save energy by not investing in electron-conductive structures, and thus investing more energy in other biological functions, such as cell division or metabolic processes. Improved electron transfer due to Ni addition may further explain the accelerated formate production observed here, as a decrease in lag phase has been previously shown for biological reactors supplemented with conductive materials.[75,77,78] While the effect of Ni on electrode conductivity and charge transfer resistance was not measured in this study, a positive correlation between dissolved Ni concentration and acetate production (Table 3) supports this mechanism of interaction between Ni and MES microorganisms, either due to improved electron transfer between the electrode and the biofilm, or due to the bio-crystalized Ni structures within the biofilm (Fig. 8).

Conclusions

In this manuscript, nickel doping on carbonaceous electrodes at low and high concentrations is shown to positively affect MES. This is the first report of concentration-dependent effects of nickel addition on MES. Factors that have been previously proposed to explain the effect of nickel on MES, such as the electrode surface area and porosity, were not found to be significant in the present study. Instead, the catalytic activity and metal concentration were highlighted as the main contributing factors for the observed effects.

High nickel loading resulted in the highest biofilm formation, acetate production and electron recovery to acetate. This was likely due to the improved H_2 production, as well as the improved charge transfer within the biofilm. Fast consumption of H_2 near the cathode surface likely resulted in the low abundance of planktonic microorganisms, due to substrate depletion. A shift from planktonic to biofilm growth may also be due to high nickel concentration in the

This journal is © The Royal Society of Chemistry 2022

Catal. Sci. Technol., 2022, **12**, 2500–2518 | **2515**

electrolyte, as a response of microorganisms to stressful conditions (*i.e.*, potential toxic effects of nickel). Large nickel deposits on the biofilm indicate that microorganisms used the available metal to create conductive bio-structures, as has been previously shown for palladium, and these may have resulted in improved electron transfer within the biofilm, and thus biofilm formation.

Low nickel loading resulted in improved acetate production and electron recovery, compared to control experiments, as well as the highest abundance of planktonic microorganisms. This was likely due to the higher availability of nickel as a trace element.

Contrary to previous reports, which only show an effect of metal addition on acetate production rate, both the rate and electron recovery to acetate were improved by nickel doping on AC in this study. Furthermore, an acceleration of formate production was observed with increasing nickel loading. These effects are likely related to the altered microbial community composition as a result of nickel addition. Altered gene expression and improved charge transfer may further explain these findings, although these factors were not investigated in the present study.

A combination of the aforementioned mechanisms (*i.e.*, catalytic activity, charge transfer, toxicity, trace element availability) of nickel interaction with MES microorganisms is evidently responsible for the observed improvement in MES performance. Therefore, the individual and combined effects of nickel on MES ought to be better understood. Multi-factorial investigations such as the present study could offer a valuable starting point for understanding the improvement of MES *via* electrode modification, both in terms of fundamental research and application.

Author contributions

Konstantina-Roxani Chatzipanagiotou: conceptualization, data curation, formal analysis, investigation, methodology, project administration, supervision, validation, visualization, writing – original draft, writing – review & editing. Ludovic Jourdin: conceptualization, methodology, project administration, resources, supervision, writing – review & editing. Johannes H. Bitter and David P. B. T. B. Strik: conceptualization, funding acquisition, methodology, project administration, resources, supervision, writing – review & editing.

Conflicts of interest

There are no conflicts to declare.

Acknowledgements

Notes and references

1 P. L. Tremblay and T. Zhang, *Biotechnol. Biofuels*, 2015, **6**, DOI: 10.3389/fmicb.2015.00201.

2 L. Jourdin, Y. Lu, V. Flexer, J. Keller and S. Freguia, *ChemElectroChem*, 2016, **3**, 581.

3 O. Choi and B. I. Sang, *Biotechnol. Biofuels*, 2016, **9**, DOI: 10.1186/s13068-016-0426-0.

4 M. Rosenbaum, F. Aulenta, M. Villano and L. T. Angenent, *Bioresour. Technol.*, 2011, **102**, 324.

5 T. Zhang, H. Nie, T. S. Bain, H. Lu, M. Cui, O. L. Snoeyenbos-West, A. E. Franks, K. P. Nevin, T. P. Russell and D. R. Lovley, *Energy Environ. Sci.*, 2013, **6**, 217.

6 H. Zhu, Z. Dong, Q. Huang, T. S. Song and J. Xie, *RSC Adv.*, 2019, **9**, 34095.

7 H. Nie, T. Zhang, M. Cui, H. Lu, D. R. Lovley and T. P. Russell, *Phys. Chem. Chem. Phys.*, 2013, **15**, 14290.

8 S. Tian, H. Wang, Z. Dong, Y. Yang, H. Yuan, Q. Huang, T. S. Song and J. Xie, *Biotechnol. Biofuels*, 2019, **12**, DOI: 10.1186/s13068-019-1413-z.

9 F. Kracke, A. B. Wong, K. Maegaard, J. S. Deutzmann, M. K. A. Hubert, C. Hahn, T. F. Jaramillo and A. M. Spormann, *Commun. Chem.*, 2019, **2**, DOI: 10.1038/s42004-019-0145-0.

10 L. Wang, Z. He, Z. Guo, T. Sangeetha, C. Yang, L. Gao, A. Wang and W. Liu, *J. Power Sources*, 2019, **444**, DOI: 10.1016/j.jpowsour.2019.227306.

11 K. R. Kim, J. Kang and K. J. Chae, *Int. J. Hydrogen Energy*, 2017, **42**, 27623.

12 L. F. Wu, C. Navarro, K. de Pina, M. Quénard and M. A. Mandrand, *Environ. Health Perspect.*, 1994, **102**, 297.

13 B. J. Kim, J. H. Park, T. H. Park, P. A. Bronstein, D. J. Schneider, S. W. Cartinhour and M. L. Shuler, *Appl. Environ. Microbiol.*, 2009, **75**, 2720.

14 R. K. Thauer, A. K. Kaster, M. Goenrich, M. Schick, T. Hiromoto and S. Shima, *Annu. Rev. Biochem.*, 2010, **79**, 507.

15 D. R. Meyer-Dombard, E. L. Shock and J. P. Amend, *Extremophiles*, 2012, **16**, 317.

16 B. Ünal, V. R. Perry, M. Sheth, V. Gomez-Alvarez, K.-J. Chin and K. Nüsslein, *Front. Microbiol.*, 2012, **3**, DOI: 10.3389/fmicb.2012.00175.

17 N. Chakraborty, M. Chatterjee, G. M. Sarkar and S. C. Lahiri, *Bioenergy Res.*, 2010, **3**, 314.

18 L. M. Paulo, A. J. M. Stams and D. Z. Sousa, *Rev. Environ. Sci. Biotechnol.*, 2015, **14**, 537.

19 M. Sarioglu, S. Akkoyun and T. Bisgin, *Desalin. Water Treat.*, 2010, **23**, 55.

20 M. Vahedi, N. Hosseini-Jazani, S. Yousefi and M. Ghahremani, *Iran. J. Microbiol.*, 2017, **9**, 160.

21 M. Anke, B. Groppel, H. Kronemann and M. Grün, *IARC Sci. Publ.*, 1984, **53**, 339.

22 V. Vij, S. Sultan, A. M. Harzandi, A. Meena, J. N. Tiwari, W.-G. Lee, T. Yoon and K. S. Kim, *ACS Catal.*, 2017, **7**, 7196.

23 K. Chatzipanagiotou, L. Jourdin, C. J. N. Buisman, D. P. B. T. B. Strik and J. H. Bitter, *ChemCatChem*, 2020, **12**, 3900.

2516 | *Catal. Sci. Technol.*, 2022, **12**, 2500–2518

This journal is © The Royal Society of Chemistry 2022

24 L. Jourdin, T. Grieger, J. Monetti, V. Flexer, S. Freguia, Y. Lu, J. Chen, M. Romano, G. G. Wallace and J. Keller, *Environ. Sci. Technol.*, 2015, **49**, 13566.

25 L. Jourdin, S. M. T. Raes, C. J. N. Buisman and D. P. B. T. B. Strik, *Front. Energy Res.*, 2018, **6**, DOI: 10.3389/fenrg.2018.00007.

26 K. J. J. Steinbusch, H. V. M. Hamelers and C. J. N. Buisman, *Water Res.*, 2008, **42**, 4059.

27 S. M. de Smit, K. D. de Leeuw, C. J. N. Buisman and D. P. B. T. B. Strik, *Biotechnol. Biofuels*, 2019, **12**, DOI: 10.1186/s13068-019-1468-x.

28 C. Sandford, M. A. Edwards, K. J. Klunder, D. P. Hickey, M. Li, K. Barman, M. S. Sigman, H. S. White and S. D. Minteer, *Chem. Sci.*, 2019, **10**, 6404.

29 S. Jain, H. M. Dietrich, V. Müller and M. Basen, *Front. Microbiol.*, 2020, **11**, DOI: 10.3389/fmicb.2020.00059.

30 S. A. Sherif, F. Barbir and T. N. Veziroglu, *J. Sci. Ind. Res.*, 2003, **62**, 46.

31 S. E. McBirney, K. Trinh, A. Wong-Beringer and A. M. Armani, *Biomed. Opt. Express*, 2016, **7**, 4034.

32 A. Vintiloiu, M. Boxriker, A. Lemmer, H. Oechsner, T. Jungbluth, E. Mathies and D. Ramhold, *Chem. Eng. J.*, 2013, **223**, 436.

33 J. He, A. Huang, N. J. J. Johnson, K. E. Dettelbach, D. M. Weekes, Y. Cao and C. P. Berlinguette, *Inorg. Chem.*, 2018, **57**, 14624.

34 J. Li, Y. Gao, K. Han, J. Qi, M. Li and Z. Teng, *Sci. Rep.*, 2019, **9**, DOI: 10.1038/s41598-019-53869-w.

35 K. L. Milliken and T. Olson, *AAPG Special Volumes, Memoir 112: Imaging Unconventional Reservoir Pore Systems*, 2016, DOI: 10.1306/13592013M112252.

36 K. Chatzipanagiotou, V. Soekhoe, L. Jourdin, C. J. N. Buisman, J. H. Bitter and D. P. B. T. B. Strik, *ChemPlusChem*, 2021, **86**, 763.

37 M. Hackbarth, T. Jung, J. E. Reiner, J. Gescher, H. Horn, A. Hille-Reichel and M. Wagner, *Chem. Eng. J.*, 2020, **390**, DOI: 10.1016/j.cej.2020.124604.

38 P. Gikas, *J. Hazard. Mater.*, 2008, **159**, 187.

39 J. H. Tian, R. Lacroix, E. D. le Quéméner, C. Bureau, C. Midoux and T. Bouchez, bioRxiv, 2019, DOI: 10.1101/609909.

40 H. Sträuber, M. Schröder and S. Kleinsteuber, *Energy Sustain. Soc.*, 2012, **2**, DOI: 10.1186/2192-0567-2-13.

41 L. Chatellard, E. Trably and H. Carrère, *Bioresour. Technol.*, 2016, **221**, 541.

42 S. Esquivel-Elizondo, Z. E. Ilhan, E. I. Garcia-Peña and R. Krajmalnik-Brown, *mSystems*, 2017, **2**, e00051, DOI: 10.1128/mSystems.00051-17.

43 X. Zhu, Y. Zhou, Y. Wang, T. Wu, X. Li, D. Li and Y. Tao, *Biotechnol. Biofuels*, 2017, **10**, DOI: 10.1186/s13068-017-0788-y.

44 Q. Liu, Z. J. Ren, C. Huang, B. Liu, N. Ren and D. Xing, *Biotechnol. Biofuels*, 2016, **9**, DOI: 10.1186/s13068-016-0579-x.

45 D. Zheng, H. Z. Wang, M. Gou, M. K. Nobu, T. Narihiro, B. Hu, Y. Nie and Y. Q. Tang, *Appl. Microbiol. Biotechnol.*, 2019, **103**, 8631.

46 X. Wei, J. Qin, Y. Shuai, K. Liu, Y. Luo, Y. Shi and S. Zhang, *Pet. Explor. Dev.*, 2012, **39**, 539.

47 R. Gross, J. Simon, F. Theis and A. Kröger, *Arch. Microbiol.*, 1998, **170**, 50.

48 S. M. da Silva, S. S. Venceslau, C. L. V. Fernandes, F. M. A. Valente and I. A. C. Pereira, *Antonie van Leeuwenhoek*, 2008, **93**, 381.

49 T. Ezaki, *Bergey's Manual of Systematics of Archaea and Bacteria*, Wiley, New York, 2015.

50 C. Perrin, R. Briandet, G. Jubelin, P. Lejeune, M. A. Mandrand-Berthelot, A. Rodrigue and C. Dorel, *Appl. Environ. Microbiol.*, 2009, **75**, 1723.

51 J. Wang, G. Li, H. Yin and T. An, *Environ. Res.*, 2020, **185**, DOI: 10.1016/j.envres.2020.109451.

52 E. M. Burkhardt, S. Bischoff, D. M. Akob, G. Büchel and K. Küsel, *Appl. Environ. Microbiol.*, 2011, **77**, DOI: 10.1128/AEM.02085-10.

53 J. Sitte, K. Pollok, F. Langenhorst and K. Küsel, *Geomicrobiol. J.*, 2013, **30**, 36.

54 J. Sitte, S. Löffler, E.-M. Burkhardt, K. C. Goldfarb, G. Büchel, T. C. Hazen and K. Küsel, *Environ. Sci. Pollut. Res.*, 2015, **22**, 19326.

55 J. Wu, J. Gao, D. Zhang, F. Tan, J. Yin, Y. Wang, Y. Sun and E. Li, *J. Oceanol. Limnol.*, 2020, **38**, 378.

56 M. Siegert, X. F. Li, M. D. Yates and B. E. Logan, *Front. Microbiol.*, 2015, **5**, DOI: 10.3389/fmicb.2014.00778.

57 J. Rui, J. Li, S. Zhang, X. Yan, Y. Wang and X. Li, *Biotechnol. Biofuels*, 2015, **8**, DOI: 10.1186/s13068-015-0339-3.

58 T. Ito, K. Yoshiguchi, H. D. Ariesyady and S. Okabe, *ISME J.*, 2011, **5**, 1844.

59 R. Cord-Ruwisch, H.-J. Seitz and R. Conrad, *Arch. Microbiol.*, 1988, **149**, 350.

60 B. S. Rajagopal and J. LeGall, *Appl. Microbiol. Biotechnol.*, 1989, **31**, 1541.

61 C. Greening, R. Geier, C. Wang, L. C. Woods, S. E. Morales, M. J. McDonald, R. Rushton-Green, X. C. Morgan, S. Koike, S. C. Leahy, W. J. Kelly, I. Cann, G. T. Attwood, G. M. Cook and R. I. Mackie, *ISME J.*, 2019, **13**, 2617.

62 F. R. Bengelsdorf, M. H. Beck, C. Erz, S. Hoffmeister, M. M. Karl, P. Riegler, S. Wirth, A. Poehlein, D. Weuster-Botz and P. Dürre, *Advances in Applied Microbiology*, Elsevier, Cambridge, 2018, vol. 103.

63 X. Wu, F. Zhao, N. Rahunen, J. R. Varcoe, C. Avignone-Rossa, A. E. Thumser and R. C. T. Slade, *Am. Ethnol.*, 2011, **123**, 447.

64 M. J. Capeness, M. C. Edmundson and L. E. Horsfall, *New Biotechnol.*, 2015, **32**, 727.

65 H. Li, J. Chang, P. Liu, L. Fu, D. Ding and Y. Lu, *Environ. Microbiol.*, 2015, **17**, 1533.

66 P. Liu, P. Liang, Y. Jiang, W. Hao, B. Miao, D. Wang and X. Huang, *Appl. Energy*, 2018, **216**, 382.

67 G. B. Diekert, E. G. Graf and R. K. Thauer, *Arch. Microbiol.*, 1979, **122**, 117.

68 D. H. Park and J. G. Zeikus, *Biotechnol. Bioeng.*, 2003, **81**, 348.

69 D. A. Lowy, L. M. Tender, J. G. Zeikus, D. H. Park and D. R. Lovley, *Biosens. Bioelectron.*, 2006, **21**, 2058.

70 L. Zhuang, S. Zhou, Y. Wang, C. Liu and S. Geng, *Biosens. Bioelectron.*, 2009, **24**, 3652.

This journal is © The Royal Society of Chemistry 2022

Catal. Sci. Technol., 2022, **12**, 2500–2518 | **2517**

71 J. E. Mink, J. P. Rojas, B. E. Logan and M. M. Hussain, *Nano Lett.*, 2012, **12**, 791.

72 K. P. Nevin, S. A. Hensley, A. E. Franks, Z. M. Summers, J. Ou, T. L. Woodard, O. L. Snoeyenbos-West and D. R. Lovley, *Appl. Environ. Microbiol.*, 2011, **77**, 2882.

73 A. Singh, B. Müller and A. Schnürer, *Sci. Rep.*, 2021, **11**, DOI: 10.1038/s41598-021-92658-2.

74 Y. Feng, Y. Zhang, X. Quan and S. Chen, *Water Res.*, 2014, **52**, 242.

75 Q. Yin, K. He, A. Liu and G. Wu, *Appl. Microbiol. Biotechnol.*, 2017, **101**, 3929.

76 Q. Yin, S. Yang, Z. Wang, L. Xing and G. Wu, *Chem. Eng. J.*, 2018, **333**, 216.

77 L. Liang, C. Sun, Z. Jin, M. Wang, Q. Yu, Z. Zhao and Y. Zhang, *Chem. Eng. J.*, 2022, **428**, DOI: 10.1016/j.cej.2021.132004.

78 C. Luo, F. Lü, L. Shao and P. He, *Water Res.*, 2015, **68**, 710.

79 Z. Zhao, Y. Zhang, Y. Li, Y. Dang, T. Zhu and X. Quan, *Chem. Eng. J.*, 2017, **313**, 10.

80 T. Tian, S. Qiao, X. Li, M. Zhang and J. Zhou, *Bioresour. Technol.*, 2017, **224**, 41.

81 Z. Zhao, Y. Zhang, X. Quan and H. Zhao, *Bioresour. Technol.*, 2016, **200**, 235.

82 F. Liu, A.-E. Rotaru, P. M. Shrestha, N. S. Malvankar, K. P. Nevin and D. R. Lovley, *Energy Environ. Sci.*, 2012, **5**, 8982.

2518 | *Catal. Sci. Technol.*, 2022, **12**, 2500–2518

This journal is © The Royal Society of Chemistry 2022